MASTERARBEIT

Titel der Masterarbeit

"Stream network-scale patterns of CO$_2$-evasion"

verfasst von

Sabrina Hengsberger, BSc

Angestrebter akademischer Grad

Master of Science (MSc)

Wien, 2013

Abstract

The relevance of inland waters for global carbon fluxes is becoming increasingly recognized. While data on local CO_2 evasion from individual lakes and streams are now becoming available at fast pace, we still lack methods to upscale these local fluxes to the landscape and eventually to entire fluvial networks. I measured and predicted CO_2 evasion in a pre-alpine fluvial network (Ybbs River, Austria) draining a 6th-order catchment (ca 400 km^2). Measurements of partial pressure of CO_2 in more than 100 streams showed CO_2 supersaturation throughout the entire network and distinct diurnal patterns. Furthermore, using whole-stream propane injections, I assessed K_{CO2}, the CO_2 transfer coefficient, along with various hydrogeomorphological parameters in 20 streams. I found a significant negative correlation between K_{CO2} values and stream discharge, which was used to predict K_{CO2} for all study streams. Furthermore, I used a suite of optical parameters that describe dissolved organic carbon properties to explain some of the spatial variation in pCO_2 within the fluvial network.

Acknowledgements

Table of Contents

1. Introduction

1.1. The role of inland waters for the global carbon cycle

Inland waters link terrestrial landscapes including soils and groundwater with oceans and the atmosphere. The earth's surface is covered by inland waters – encompassing lakes, ponds, rivers, streams, wetlands and reservoirs – by only 1%, but their contribution to global carbon (C) fluxes should not be underestimated (Battin, Luyssaert et al. 2009). Atmospheric carbon dioxide (CO_2) concentrations already increased from approximately 280 parts per million (ppm) before industrial revolution, to more than 384 ppm in 2008 (Battin, Luyssaert et al. 2009).

Stream ecosystem respiration (ER) and gross primary production (GPP) constitute the C fluxes in streams and rivers linked to organismic metabolism. GPP is the amount of organic C produced by photosynthesis of phytoplankton, benthic microbial autotrophs and macrophytes. This organic matter is of autochthonous origin, i.e. it is produced within the stream or river. In contrast, allochthonous organic matter enters the river as leaf fall from riparian vegetation or with soil water, for instance. Both allochthonous and autochthonous C support the respiration (R) of microbes and animals, which in oxygenated environments essentially is an oxidation to CO_2. Along this pathway, heterotrophic biota respire approximately 1.2 Pg of terrestrial C yr^{-1} and release it to the atmosphere (Battin, Kaplan et al. 2008). Generally, ER exceeds GPP in freshwater ecosystems and particular fluvial networks, because ER is additionally fueled by allochthonous organic matter inputs. This results in a global net ecosystem production (NEP=GPP-ER) of -0.12 Pg C yr^{-1}, hence fluvial networks are heterotrophic systems responsible for a net export of C from terrestrial ecosystems to the oceans and to the atmosphere (Cole and Caraco 2001; Battin, Kaplan et al. 2008; Demars, Manson et al. 2011).

During the last years several studies have highlighted that this aquatic export of terrestrially derived C in the terrestrial C balance and inland waters have emerged as playing an important role in sequestration, mineralization and transportation of C (Cole 2007; Battin, Luyssaert et al. 2009; Johnson, Billett et al. 2010).

Another estimation is shown in Figure 1, where 1.9 Pg C yr^{-1} of terrestrial net ecosystem production is exported to inland waters, where about 0.23 Pg C yr^{-1} are stored in sediments or buried in lakes. Lotic systems like streams and rivers transport 0.9 Pg C yr^{-1} to the oceans and an amount of 0.75 Pg C yr^{-1} is emitted to the atmosphere as CO_2 (Cole 2007).

Recently updated estimations even suggest that inland waters transport mineralize and bury a total amount of approximately 2.7 Pg C yr^{-1}, which is similar to the terrestrial C sink for anthropogenic emissions of 2.8 Pg C yr^{-1}. This indicates that inland waters play an active and therefore important role in the global C cycle (Battin, Luyssaert et al. 2009).
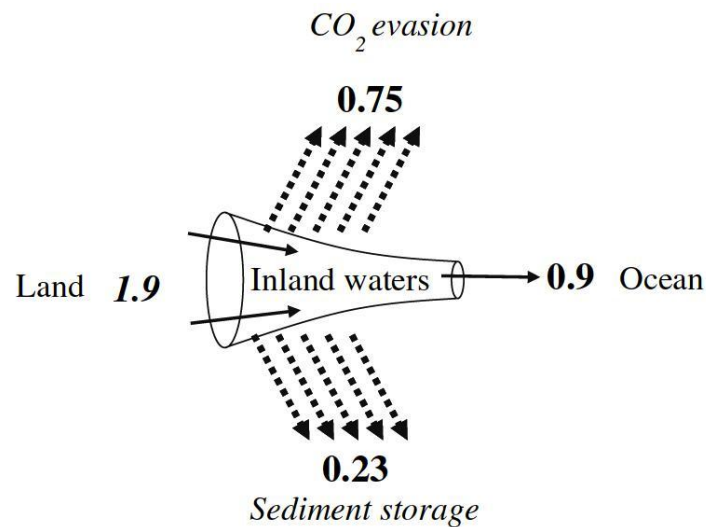
Figure 1: The role of inland waters in the global C cycle, numbers are C fluxes in Pg C yr^{-1} (Cole and Caraco 2001).

1.2. Streams and rivers

C-fluxes in streams are 3-dimensional. On the one hand there is a vertical loss of C as CO_2 or CH_4 and on the other hand C is transported downstream as particulate organic C (Füreder and Pöckl 2007), dissolved organic carbon (Leopold and Maddock 1953) or dissolved inorganic carbon (DIC) (Wallin, Buffam et al. 2010). Most of the C transported in streams and rivers is returned to the atmosphere as CO_2 before reaching the oceans or being stored within river corridors as sedimentary organic carbon (OC) after erosion and transport from distant sites (Aufdenkampe, Mayorga et al. 2011).

Nearly all fresh waters have supersaturated CO_2 concentrations with respect to concentrations of CO_2 in the atmosphere. The partial pressure of dissolved CO_2 (pCO_2) in water in equilibrium with the atmosphere is equivalent to the concentration of CO_2 in the atmosphere, which is currently about 390 ppm by volume (Cole and Caraco 2001; Humborg, Morth et al. 2010). The supersaturated CO_2 concentrations in fresh waters implicate high freshwater-to-atmosphere CO_2 fluxes (Cole and Caraco 2001), which must be balanced by inputs from terrestrial systems, as either OC- or CO_2-rich groundwater (Mayorga et al. 2005; Johnson et al. 2008).

1.3. The spatial structure of riverine ecosystems

The important role of streams and rivers in the global C cycle is mostly based on their unique spatial structure. The dendritic network structure of riverine systems allows most efficient hydrological

drainage of the landscape, leading to collection of organic as well as inorganic C entering riverine ecosystems mainly through headwater streams and groundwater seepage (Brown, Swan et al. 2011). The gradient in ecological conditions along the riverine continuum from headwaters to larger rivers has been recognized as an important control on ecosystem metabolism in the seminal "River Continuum Concept" (RCC) (Vannote, Minshall et al. 1980): This concept describes the structure and function of communities along the riverine continuum. Basically it proposes to consider the gradient of physical factors formed by the increasing stream/river size for understanding biological strategies of organisms and the metabolic dynamics of the whole fluvial ecosystem. Thus, fluvial geomorphological processes regulate energy input, organic matter transport, storage and use by higher organisms like macroinvertebrates with specific feeding strategies. Physical variables within a stream present a continuous gradient of conditions such as width, depth, velocity, flow volume and temperature. Headwater streams are strongly influenced by the riparian vegetation which reduces autotrophic production by shading and also contributes large amounts of allochthonous detritus. Terrestrial organic input becomes less important as stream size increases, while autochthonous primary production and organic C transported from upstream increase in importance as resources. This creates a gradient in the ratio of GPP to R from headwaters to large rivers. GPP:R is less than 1 in headwater streams. In medium-sized streams primary production increases, the ratio is more than 1 (GPP:R>1) because of more light availability. Large rivers are characterized by GPP:R<1 because of increased depth and turbidity due to fine particulate organic matter from upstream limiting primary production.

As mentioned above, the RCC first predicts an increase in autotrophic processes in a downstream direction due to increased light penetration as streams become wider. Empirical data confirms this assumption using chlorophyll *a* as an indicator for benthic primary production (Minshall, Thomas et al. 2000): Chlorophyll *a* concentrations were lowest in headwater streams and greatest in farthest downstream reaches.

Other data (Lamberti and Steinman 1997) confirms and extends the hypotheses of the RCC showing higher GPP in small to medium-sized streams in unforested landscapes, where lower canopy cover allows photosynthesis without light limitation. In contrast, small streams in more forested areas had lower GPP, while large and deep rivers had medium GPP due to reduced shading by vegetation on the one hand but light attenuation by the dissolved and suspended load of water on the other hand.

As the RCC suggests, streams and rivers are not enclosed ecosystems. They should be regarded as a "meta-ecosystem", a set of ecosystems which is connected by spatial flows of energy, materials and organisms across ecosystem boundaries (Loreau, Mouquet et al. 2003). Flows of inorganic elements, living and dead organisms can influence the functioning of local ecosystems but they can also create interdependence between local ecosystems operating as global constraints at the scale of the meta-

ecosystem. The "meta-ecosystem" has led to an understanding of streams and rivers as three-dimensionally connected ecosystems, which on the one hand experience enormous vertical and lateral exchange and on the other hand evolve along a longitudinal continuum (Battin, Kaplan et al. 2008).

Further, the dendritic network structure of streams and rivers must be considered, as it is shown to be important, for instance, at river confluences, which are high-quality habitats. For example disturbances induced by flooding occur more frequently in confluences and they provide most dynamic and complex biophysical habitats. Thus, river confluences create more habitat heterogeneity in river ecosystems (Osawa, Mitsuhashi et al. 2010).

Indeed, river networks are dendritic ecological networks (DENs) (Grant, Lowe et al. 2007) where ecological processes such as dispersal or community interactions take place in the branches themselves, while nodes serve as transfer points where branch dynamics are modified.

Also food webs are affected by drainage networks, for example insectivorous bats are deterred from headwater hunting because of the splashing water in steep reaches which interferes with their ultrasonic foraging calls. While their day roost is located near headwaters, they move many kilometers downstream for hunting (Power and Dietrich 2002).

1.4. DOM – the fuel for heterotrophic metabolism in streams and rivers

Dissolved organic matter (DOM) is the largest pool of organic C on earth as well as the largest fraction of organic C in streams and rivers, its quantity is usually measured as bulk dissolved organic C (Leopold and Maddock 1953). Terrestrially derived C can enter an aquatic ecosystem also as POC (Füreder and Pöckl 2007), which is defined as organic C larger than 0.63 µm, whereas DOC is smaller than 0.63 µm. While DOC is transported with the water, POC also settles via gravitation and drag forces due to its larger size and mass. Since POC is not significantly transported downstream, it tends to be consumed locally and quickly (Cummins 1974). DOC receives more attention as it is the intermediary with the global C cycle (Battin, Kaplan et al. 2008). In aquatic ecosystems DOM controls light attenuation and influences metal speciation and bioavailability, it may also act as pH buffer (Cory and McKnight 2005) and certainly serves as a source of energy and nutrients to the aquatic food web.

In fact, DOM is the main energy source for heterotrophic organisms in rivers and streams, and it consists of thousands of different chemical compounds with aromatic and aliphatic hydrocarbon structures. This heterogeneous mixture resulting from the production and the breakdown of bacterial, algal and higher plant organic material includes organic materials like humic substances

(humic and fulvic acids), hydrophilic acids, amino acids, carboxylic acids, proteins, lipids and hydrocarbons. Humic substances cause a yellow-brown color and have a high molecular weight, they are refractory anionic macromolecules containing aromatic and aliphatic components (Aiken and Leenheer 1993). The relative concentrations of the multiple DOM compounds vary because of the high variety of chemical and biological production and degradation processes of animals and plants (Thurman 1985; Kaplan and Newbold 2003; Cory and McKnight 2005).

About 20-40% of the DOC in natural water consist of transphilic acids, amino acids, carbohydrates and proteins. This non-humic hydrophilic fractions of DOM are less hydrophobic and form the lower molecular weight DOC (Aiken and Leenheer 1993; Owen, Amy et al. 1995).

Also carbohydrates are an important reactive fraction of DOM in water and exist in classes like monosaccharides, oligosaccharides, polysaccharides and saccharides. Bound to humic substances they can be linked together into polymers to several important polymeric sugars. Amines and amides are derived from amino acids, polypeptides and aquatic humic substances.

While the lower molecular weight fraction of DOM is an important substrate for heterotrophs, the low molecular weight organic acids represent the degradation products of organics released by algae and bacteria as a result of chemical and biological oxidation processes (Owen, Amy et al. 1995).

The fraction of DOM that absorbs UV and visible light is defined as chromophoric or colored DOM (CDOM) and plays an important role in many chemical and biological processes in aquatic ecosystems such as shielding biota from harmful UV-radiation. In inland waters CDOM mostly originates from lignocellulose of plant support tissues and contains large quantities of humic and fulvic acids. CDOM is also produced by degradation of microbial and algal biomass (Helms, Stubbins et al. 2008; Loiselle, Bracchini et al. 2009). The origin of DOM influences its spectral absorption and its resistance to photochemical and biological degradation, and degradation processes themselves may again alter its optical properties (Vodacek, De Grandpre et al. 1997; Del Vecchio and Blough 2004). Changes in absorption have also been associated with losses in aromaticity and humification (Weishaar, Aiken et al. 2003). Source and composition of DOM show spatial and temporal variability due to hydrological, biotic and biogeochemical factors, and also as a result of anthropogenic influences (Amon and Benner 1996).

The enormous chemical diversity of DOM has only recently been recognized due to the application of high-resolution analytical techniques, such as FT-ICR-MS (Fourier Transform Ion Cyclotron Resonance Mass Spectroscopy) or LC-MS (Liquid Chromatography Mass Spectroscopy). FT-ICR-MS of DOM produces mass spectra that can be used to estimate molecular weight, identify patterns of elemental

composition and calculate weighted H:C and O:C ratios (Seitzinger, Hartnett et al. 2005; Hertkorn, Frommberger et al. 2008).

A range of studies has used simpler approaches to determine important chemical classes or deliver proxies for chemical characteristics of DOM, among these are absorbance-spectrophotometry and fluorescence-spectrophotometry (Thurman 1985; Kim, Simpson et al. 2003; Kim, Kaplan et al. 2006). UV absorbance measurements via absorbance spectrophotometry provide an estimation of the organic C content in the samples. Fluorescence is another property of DOM which is easily measured, providing information about the source, redox state and biological reactivity of DOM (Fellmann, Hood et al. 2010). Three-dimensional excitation-emission spectroscopy is generally used to identify fluorescent compounds in complex mixtures (Parlanti, Worz et al. 2000). Fluorescence-spectrophotometry is a relatively rapid technique to characterize DOM, the molecules in the sample are excited by light and release energy in the form of light (fluorescence) which can be measured. It is also possible to create a 3D picture by measuring the fluorescence intensity at each point in a matrix of excitation and emission wavelengths, yielding an excitation-emission-matrix (EEM). Fluorescence data can indicate chemical properties of humic substances and distinguish DOM from different origins, such as microbial DOM from terrestrial DOM (McKnight, Boyer et al. 2001; Kaplan and Newbold 2003; Cory and McKnight 2005).

Another increasingly important but simple tool to study DOM are DOC-bioassays which measure biodegradable carbon (BDOC) – a conventional measurement for biodegradable organic matter (BDOM). This is the fraction of DOM that can be used by microorganisms as a source of energy and nutrients. The bioavailability of DOC in streams is affected by hydrodynamics, retention times and streambed microbial activity. This part of DOC can be determined by the difference in initial and final concentration of DOC after incubation with a native or standard microbial population. Due to the lack of analytical methods and the complexity of BDOC little is known about its composition. But knowing the components of BDOC helps to understand how heterotrophic bacteria obtain energy and nutrients (Kaplan and Newbold 2003; Camper 2004; Lyon and Ziegler 2009).

Absorbance spectrophotometry provides a number of parameters to describe DOM quality:

- $SUVA_{254}$: The Specific UV Absorbance is defined as the UV absorbance of a water sample at a wavelength of 254 nm normalized for dissolved organic C concentration (DOC in mg L^{-1}). Low SUVA values indicate non-humic substances such as proteins, while high SUVA values indicate more humic DOC (Weishaar, Aiken et al. 2003; Helms, Stubbins et al. 2008).

- E2:E3 is a ratio of absorbance coefficients that gives information about aromaticity and molecular weight of DOM (De Haan and De Boer 1987; Peuravuori and Pihlaja 1997; Helms, Stubbins et al. 2008; Hillebrand, Borer et al. 2009).

- Another ratio is E4:E6, it correlates inversely with DOM aromaticity and also with molecular size, O:C, C:N, carboxyl content and total acidity. E4:E6 can be used as general indicator of humification (Peuravuori and Pihlaja 1997).

- The slope parameter S describes CDOM composition because it is correlated with the ratio of fulvic to humic acids and also shows correlation with the molecular weight of fulvic acids (Twardowski, Boss et al. 2004; Helms, Stubbins et al. 2008).

- S_R: The slope ratio is inversely correlated with molecular weight of DOM and has been identified as indicator of photodegradation (Helms, Stubbins et al. 2008).

Fluorescence-based excitation-emission matrices (EEMs) yield indicators of recently produced and microbially derived DOM, terrestrially derived DOM and humification. Some parameters are:

- The peak ratio β:α as an indicator for autochthonous vs. allochthonous DOM sources. The β-peak is regarded as a typically "microbial" peak related to autochthonous production, while α is regarded as indicating humic-like substances. β:α serves as a "freshness index" indicating the importance of recently produced DOC vs. more decomposed DOC components (Parlanti, Worz et al. 2000; Wilson and Xenopoulos 2008).

- FI: The Fluorescence index serves to distinguish sources of fulvic acids – it is higher for microbially derived, younger and autochthonous fulvic acids and lower for terrestrially derived, older and allochthonous fulvic acids (McKnight, Boyer et al. 2001).

- HI (Humification Index): There is a decreasing H:C ratio during humification which means a shift to more condensed molecules which show fluorescence at higher wavelength (De Haan and De Boer 1987).

A statistical modeling approach is applying parallel factor analysis (PARAFAC) to DOM excitation-emission matrices. This analysis allows the partitioning of EEMs into fluorophores characterized by unique excitation and emission spectra (Cory and McKnight 2005). It is a three-way method that

decomposes the fluorescence signature of DOM into individual components and provides an estimation of the relative contribution of each component to total DOM fluorescence. Thus, PARAFAC components provide information about the biochemical composition, origin, and biogeochemical role of aquatic DOM. Commonly fluorescent components are described as humic-like, fulvic-like or protein-like (also referred to as tyrosine- or tryptophan-like) because each component represents a group of fluorophores with fluorescence properties similar to those of reference materials. The advantage of PARAFAC is that a more complete analysis of EEMs is possible and additional information such as oxidation state may be obtained from the EEMs. PARAFAC can take overlapping fluorescence spectra and decompose them into defined fluorescence components (Fellmann, Hood et al. 2010).

Another important fraction of DOC is dissolved inorganic carbon (DIC), it includes CO_2, carbonic acid, bicarbonate anion and carbonate (Barnes and Raymond 2009). Terrestrial ecosystems influence DIC in streams through hydrologic transport of CO_2 produced in soils and groundwater via plant root and microbial respiration and HCO_3 – generated via weathering (Finlay 2003).

1.5. Main goals of the study

I aim to show spatial variability of DOM and hydromorphological parameters in an entire fluvial network, thereby contributing to our knowledge on the importance of streams relative to rivers. Further, I aim to understand the spatial variability of the gas transfer coefficient K_{CO2} and its physical controls, and to produce a predictive model for K_{CO2} based on physical parameters such as depth, discharge and slope. My study also includes measurements of CO_2, and as a result the study should combine CO_2 with K_{CO2} to get CO_2 evasion for all sampled streams and should finally serve as a base for realistic upscaled estimates of CO_2 evasion fluxes for the whole stream network.

Another important aspect of the study is to investigate day and night variation of CO_2 due to primary production and respiration. Sampling of all streams during day and night within a week and at identical discharge conditions provides a single complete network-wide snapshot of DOC-properties and CO_2.

2. Material and Methods

2.1. Study area, timing and overview of sample collection procedures

I studied the pre-alpine stream network of the river Ybbs in Lower Austria in the vicinity of Lunz am See (Figure 2). The network was sampled at 105 sites ranging from 1st to 6th stream order (Table 1) along the mainstem of the Ybbs (downstream of Lunz am See) and the tributaries Bodingbach, Steinbach, Ois and Seebach. The 6th order Ybbs River at the village Göstling was the lowermost downstream sampling site, which corresponds to a total catchment size of approximately 360 km². Samples were taken for CO_2 concentrations (as pCO_2) and K_{CO2} (gas transfer coefficient) was determined with the tracer gas method using propane in 20 experimental injections at sites distributed throughout the catchment. Also, hydromorphological key variables (slope, velocity, average depth and width) were measured. Furthermore water samples were taken to analyze DOC, DOM quality by optical methods, DIC and nutrients.
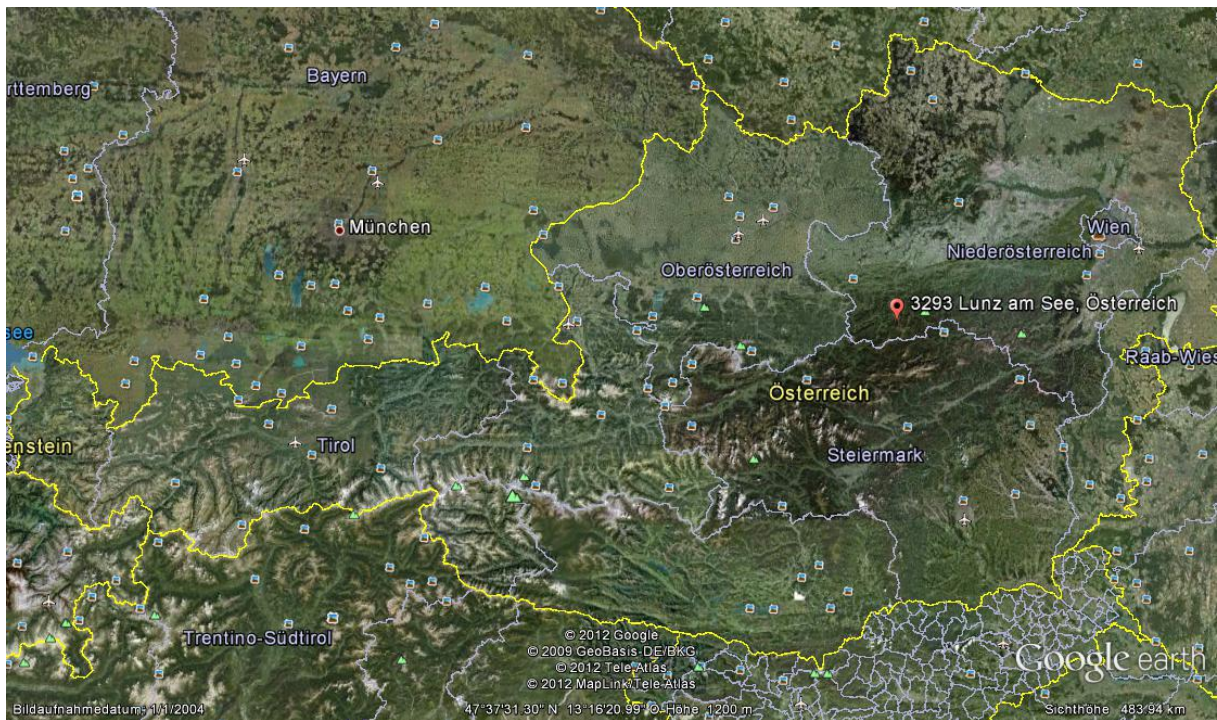

Figure 2: Lunz am See in the southwest of Lower Austria is located at latitude 47"51'22.06" N and longitude 15"01'35.04" E, the altitude is approximately 600 m.

Table 1. The 105 sampled streams ranged from 1st to 6th stream order.

Strahler stream order	Number of streams
1st	3
2nd	22
3rd	33
4th	28
5th	18
6th	1
total	**105**

The 4 tributaries form 4 geographically distinct subcatchments with altitude ranging from 531 m to 1051 m above sea level and an average altitude of 747.4 m. Sampling sites were arranged in 35 triplets at network nodes, where one triplet consisted of two adjacent tributaries and their confluence (Figure 3). The confluence was sampled slightly downstream to assure complete mixing of the tributaries. For the predominantly small and turbulent streams of our study, mixing distance was assumed to be approximately 15-25 times the average stream width (Camper 2004) and double-checked by constant conductivity across a stream transect.
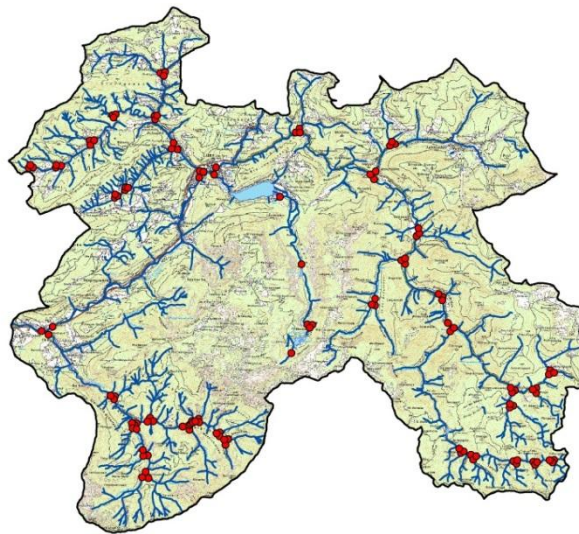
Figure 3. Overview of the stream network; triplets of sampling sites are located at 35 confluences, respectively.

The whole stream network (105 sites arranged in 35 triplets) was sampled twice (day and night) within a single week by 4 simultaneously working sampling teams in December 2010. The day sampling was restricted to ± 2 hours around astronomical noon (approximately 12:00), night sampling was restricted to 4 hours after sundown (22:00 to 1:00). These sampling times bracket the times of diurnal minimum and maximum CO_2-concentrations at the Oberer Lunzer Seebach (one of the sampling sites) where CO_2 is continuously measured by an automatic monitoring station for another study.

The hydrograph prior to and during sampling was characterized by stable baseflow conditions (Figure 4+5). We chose the timing of sampling during late fall and after a prolonged baseflow period to maximize metabolic activity due to high periphyton abundance and high allochthonous organic C inputs in the form of leaf litter.
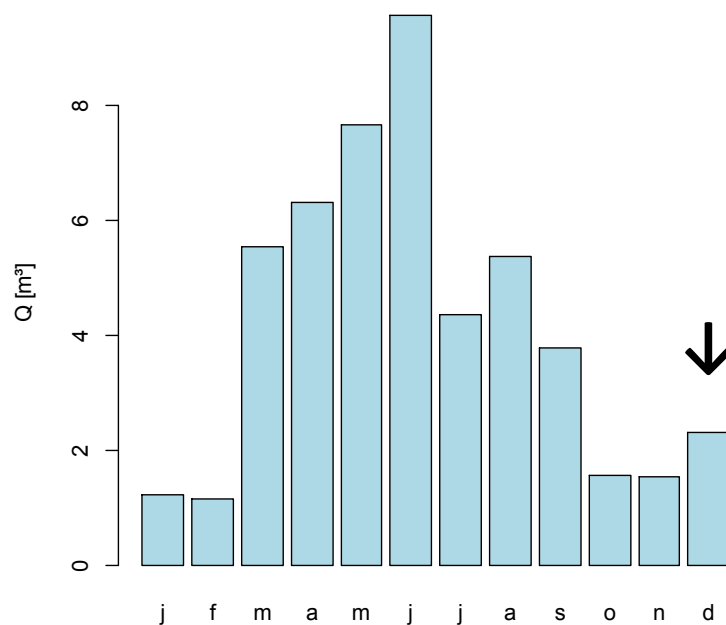
Figure 4. Continuous measurements of discharge in Lunz during 2010, the arrow signifies sampling time (data from "Amt der Niederösterreichischen Landesregierung – Abteilung Hydrologie und Geoinformation").
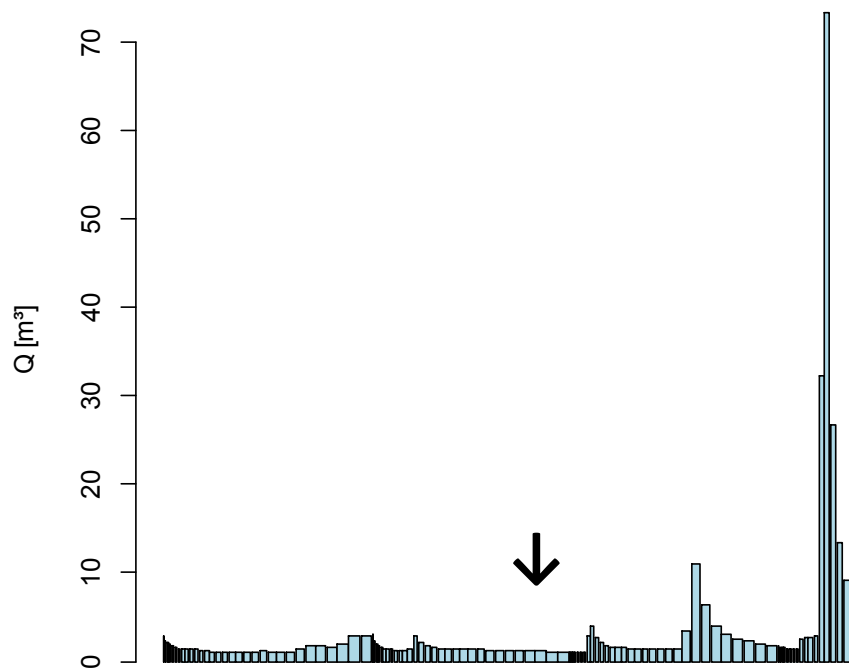
Figure 5. The data from Lunz show stable baseflow conditions before the first sampling (arrow) in December 2010 (data from "Amt der Niederösterreichischen Landersregierung – Abteilung Hydrologie und Geoinformation").

The teams collected samples for CO_2, dissolved organic and inorganic carbon (DOC and DIC) and conservative ion concentrations during both night and day. Conductivity, pH and temperature were measured on-site using portable field meters (WTW, YSI). Hydromorphological key variables (slope, velocity, average depth and width) were measured at each site for a representative stream reach once (at undefined times but at the day of water sampling). Constant discharge between night and day was assured by sampling the same site within 24 hours and controlling gauge on a temporarily installed gauging stick.

Experimental gas (propane) injections were done at 20 sampling sites and at similar hydrological conditions during 3 sampling campaigns spread through winter 2010 to 2011. Sampling sites were selected to cover the entire gradient of hydromorphological conditions existing across the 105 network sampling sites. Alongside measuring gas exchange, we measured the same hydromorphological variables as measured during the water sampling campaign to allow model building and prediction of gas exchange coefficients for all 105 sampling sites.

2.2. Water sampling

Duplicate water samples for DOC (Leopold and Maddock 1953) were collected during night and day at each stream sampling site by filtering 25 ml of stream water into acid-treated (0.1 M, overnight), washed (3 times with MQ) and combusted (4 hours, 450 °C) 30 mL glass vials through a double-layer of combusted GF/F filters mounted in a syringe filter on a 60 ml plastic syringe. Vials were closed with NaOH-pretreated (0.5 M, overnight) and MQ-washed teflon septa. The same sampling procedure was used to collect samples for optical analyses of DOM by absorbance and fluorescence spectrophotometry, except that these samples were filled in amber 30 ml vials to prevent photobleaching effects. These vials were identically prepared.

For BDOC two vials were filled with 38 mL stream water as mentioned above and 2 mL of raw stream water were added to each vial as inoculum.

Samples for DIC were collected using a 60 ml syringe and filtered through pre-rinsed 0.2 μm polycarbonate syringe filters into 40 ml combusted glass vials. To minimize gas exchange between water and air the syringe filter was fitted with a needle and care was taken to avoid bubble formation. Vials were overfilled and tightly closed without entrapped air bubbles using a single-use plastic cap with a sterile teflon septum.

For conservative ions (Na^+, K^+, Ca^{2+}, Mg^{2+}, Cl^-, NO_3, and SO_4^{2-}) one water sample per stream was filtered into sterile 20 mL Falcon tubes using a syringe fitted with a pre-rinsed 0.2 μm polycarbonate syringe filter. Ion concentrations were only determined once a day for each site, assuming similar discharge conditions and ion concentrations between day and night.

CO_2 samples were taken as described in (Harvey and Peterson 1997): Briefly, 40 mL of stream water was slowly collected into a 60 ml syringe. After adding 20 ml of ambient air the syringe was closed with a needle and shaken vigorously for 1 minute under water to achieve water-air gas equilibrium at in-situ temperature. 15 ml of the equilibrated air were then injected into evacuated 10 ml crimp-seal glass vials closed with a butyl rubber septum. The needle-piercing site in the septum was then covered with silicon paste. Two such samples were collected at each stream site. Two additional 15 mL samples of ambient air were collected for each triplicate of sites.

All water samples were stored at 4°C pending analysis.

2.3. Hydromorphology (at 105 sites)

Representative stream reaches (16 m – 150 m) were determined to measure depth, width, slope and discharge. Discharge and average velocity for the representative reach were determined by slug additions of a known mass of NaCl dissolved in stream water. The NaCl slug was added to the

streamflow at the upstream end of the representative reach and entire breakthrough curves of conductivity were automatically logged at the downstream reach end with a WTW field meter. The time difference between slug start time and the time of maximum conductivity at the stream reach end was taken as water travel time. The velocity was calculated by dividing the stream reach length through the water travel time. Stream discharge at the reach end was calculated from the integral of electrical conductivity curves corrected for background conductivity (Wallin, Öquist et al. 2011). For large rivers a method of average stream velocity and cross-sectional area was used (Gordon, McMahon et al. 2004) where Q is calculated from:

$$Q = w\bar{d}\bar{v}$$

where *w* is the width in meters at a chosen transect location and *d* and *v* are the average depth and velocity computed from multiple measurements (min n=15) across the transect. Velocity was measured at 40 % depth above the streambed in m s^{-1} using an electromagnetic flow meter (Marsh McBirney FloMate).

We measured discharge at two of three sites of each triplicate (two tributaries and confluence). The missing discharge value was calculated by combining a mass balance with conductivity measurements:

$$Q_1 + Q_2 = Q_3 \quad \text{and} \quad EC_1 * Q_1 + EC_2 * Q_2 = EC_3 * Q_3$$

where EC stands for electric conductivity and Q for discharge at sites 1, 2 and 3.

Width was measured at least 10 times per stream reach, more often in larger streams. Also, depth was measured randomly every three steps along a zig-zag pathline through the stream reach. The streambed and water surface slope were determined with hydrostatic leveling using a water level gauge filled with ink or using an optical leveling instrument in case of longer stream reaches (Gordon, McMahon et al. 2004). Missing slopes were determined from topographical maps (1:50000, BEV, AMAP 3D Fly).

Hydromorphological data of width, depth and velocity were related by modeling of hydraulic geometry (Leopold and Maddock 1953; Harvey and Peterson 1997) with the following power law expression:

$$W = a * Q^b$$

$$D = c * Q^f$$

$$U = k * Q^m$$

where W is width, D is depth and U is the velocity. Here, the coefficients a, c and k must multiply to unity as a*c*k, while the hydraulic exponents b, f and m must sum to unity as b+f+m. The fitted power law relationships were also used to predict hydromorphological data from Q in case of missing data.

2.4. Gas transfer coefficient of CO_2

The tracer gas method has been widely used to determine evasion rates for inland surface water. The method determines the gas exchange ability across the water-atmosphere interface due to injection of an inert volatile gas tracer which does not naturally occur in the water system, for example propane (C_3H_8) (Wallin, Öquist et al. 2011). Some studies have already used injections of gas tracers to measure the gas transfer coefficient for CH_4 and CO_2, but mainly focused on just one stream which has been used as the basis for regional upscaled estimates (Wanninkhof, Mulholland et al. 1990; Jones, Grey et al. 1998; Hope, Palmer et al. 2001; Oquist, Wallin et al. 2009).

The gas transfer coefficient of CO_2 (K_{CO2}) was determined by a continuous (i.e. metered) injection of propane as an inert volatile tracer and measuring downstream concentration decline in a defined experimental stream reach during steady-state injection conditions (Genereux and Hemond 1992; Marzolf, Mulholland et al. 1994; Wallin, Öquist et al. 2011). A slug injection of a conservative solute tracer (NaCl) with a known mass was done immediately prior to the propane injection 10-20 m upstream of the experimental reach. Breakthrough curves of electrical conductivity were logged with WTW or YSI conductivity meters at the start and end of the experimental reach to determine stream discharge (Q), reach travel time (τ) and velocity. Approximate reach water travel time was already determined in the field from the approximate timing of visually determined breakthrough curve conductivity maxima. Changes in discharge along the stream reach allowed correcting for any potential dilution by underground lateral inflow.

Experimental stream reaches were selected to represent the entire gradient of hydromorphological conditions existing in the 105 network sampling sites and defined in a manner to avoid visible lateral inflow and allow sufficient length for gas evasion (12 – 150 m, depending on stream size). Discharge computed from conductivity data was used for correction of dilution effects by undetected vertical or lateral inflow of water. Morphological measurements (depth, width) were done in the same manner as during the water sampling campaign and for the entire experimental reach. At many occasions stream reaches were divided up to three subreaches and all data was generated for each subreach from a single injection experiment.

Propane was bubbled into the stream through an air curtain from a 10 kg-tank. Depending upon stream size, up to three large diffusers were placed 10-20 m upstream from the start of the

experimental reach. A plastic foil cover (length 5-10 m) was placed above the diffusers and immediately downstream to prevent immediate degassing and increase propane loading of the water column. The injection was done at a constant propane flow rate achieved by a fixed pressure of 2.5-3 bar. Sampling was not started before the injection had lasted for a minimum time period corresponding to 3 times the approximate reach water travel time, this ensured sampling at steady state conditions. In order to sample the same water mass the sampling time at each spot was computed from reach travel time (Marzolf, Mulholland et al. 1994). Three replicate stream samples were taken at each stream (sub)-reach end. Each sample consisted of 10 mL stream water filled into a 22 mL glass vial using a syringe and a large-diameter needle and immediately closed with a crimp-seal cap mounted with a gas-tight PTFE-coated butyl rubber septum. Samples were stored at 4°C pending analysis by gas chromatography (Agilent gas chromatograph equipped with a Restek packed ShinCarbon column #19809 and a flame-ionization detector). Samples were equilibrated and kept at constant temperature in a water bath at 40°C. The headspace was sampled once and injected into the gas chromatograph through a 16-port multi-positioning valve. Propane peak areas were determined by automatic peak detection and integration using the Agilent ChemStation software.

The gas transfer coefficient of propane (K_{C3H8} in units of time $^{-1}$) is defined as the dilution-corrected fraction of the tracer gas that is lost over a specific reach per minute and can be calculated according to (Wallin, Öquist et al. 2011):

$$K_{C_3H_8} = \frac{1}{\tau} * \ln \frac{[C_3H_8]_U * Q_U}{[C_3 3H_8]_L * Q_L}$$

where τ is the travel time of water along the reach in minutes, $[C_3H_8]_U$ and $[C_3H_8]_L$ are the propane concentrations at the upper and lower end of the reach, Q_U and Q_L are the corresponding discharges at the upper and lower reach end in L s^{-1}. Propane peak areas as determined by gas chromatography were directly used instead of concentrations.

K_{C3H8} can be converted to K_{CO2} (Jones and Mulholland 1998; Wallin, Öquist et al. 2011):

$$K_{CO_2} = K_{C_3H_8} * \left(\frac{d_{CO_2}}{d_{C_3H_8}}\right)^n$$

where the gas diffusion coefficients d_{CO2} and d_{C3H8} are computed from the stream temperature T in °C based on (Aiken and Leenheer 1993) and (Owen, Amy et al. 1995):

$$d_{CO_2} = 0.9477 exp^{(0.0274*T)}$$

$$d_{C_3H_8} = 1.092 exp^{(0.0235*T)}$$

Due to the influence of temperature, K_{CO_2} values are normalized to 20°C (Wallin, Öquist et al. 2011):

$$K_{CO_2}(20°) = K_{CO_2}(T) * \theta^{(20-T)}$$

where T is the stream water temperature in °C, the value θ was set to 1.01 based on reaeration values in the literature (Metzger and Dobbins 1967).

Electrical conductivity, pH, O_2 concentration, atmospheric pressure and temperature were determined with field meters (WTW and YSI).

Dilution correction was made for propane values if discharge increased along an experimental reach with

$$P_1 * Q_1 = P_2 * Q_2$$

where Q_1 and Q_2 are the discharges at the end and beginning of the experimental (sub) reach and P stands for the respective propane concentrations.

2.5. Laboratory analyses

Headspace propane concentrations were analyzed with gas chromatography (GC) (Agilent gas chromatograph).
DOC was measured using a Sievers 900 TOC-analyser (GE Analytical Instruments) fitted with an inorganic carbon remover. DIC was measured with the same device at idle inorganic carbon remover by differencing total dissolved carbon and DOC.

Optical properties of DOC were measured with a Shimadzu UV-17000 Pharma Spec. spectrophotometer and a Hitachi F-7000FL diode array spectrofluorometer. Samples were acclimatized to room temperature in darkness prior to measurement.
For absorbance measurements Milli-Q water was used as a blank and absorbance scans were done for a wavelength range between 250 nm and 700 nm at 5 nm intervals using a 10 cm quartz cuvette.

Fluorescence was measured using a 1 cm quartz cuvette and as a 3D scan resulting in an excitation-emission matrix (EEM) over an emission range from 200 – 450 nm at 2 nm intervals and an excitation range of 250 – 600 nm at 5 nm intervals. Milli-Q-water served as blank, Milli-Q water and Quinonsulfate were used as standards and to monitor instrument drift (less than 1%). The scan speed was 12000 nm min^{-1}. The fluorometer recorded corrected spectra with eliminated instrumental response regarding wavelength characteristics of the monochromator and photomultiplier. Conservative cations and anions were analysed by standard ion chromotography.

2.6. Data analysis

2.6.1. DOM-optical data

The fraction of dissolved organic matter (DOM) absorbing light in the UV region is called chromophoric or colored DOM (CDOM). Measuring CDOM allowed to derive absorption-related indices that have been shown to correlate with molecular properties of DOM. Absorption spectra yielded indicators of DOM-aromaticity, average molecular weight of DOC (De Haan and De Boer 1987; Peuravuori and Pihlaja 1997; Helms, Stubbins et al. 2008), the ratio of fulvic to humic acids and photodegradation.

Absorbance data was log-transformed and absorbance coefficients were calculated with:

$$a_\lambda = \frac{2.303 * A_\lambda}{l}$$

where a_λ is a wavelength-specific absorption coefficient (m^{-1}), A_λ is the measured absorbance value and l is the path length of the cuvette (in m).

The specific UV-absorbance SUVA$_{254}$ as an indicator for DOM aromaticity and humic substances (Weishaar, Aiken et al. 2003) was computed by:

$$SUVA_{254} = \frac{a_{254}}{[DOC]}$$

where the absorption coefficient at 254 nm is given as a_{254} and DOM is the concentration of DOC in ppm.

Two commonly used ratios of absorption coefficients termed E2:E3 and E4:E6 give further information about aromaticity and molecular weight of DOM (De Haan and De Boer 1987; Peuravuori and Pihlaja 1997; Helms, Stubbins et al. 2008):

$$E2:E3 = \frac{a_{250}}{a_{365}}$$

$$E4:E6 = \frac{a_{465}}{a_{665}}$$

where a_{250}, a_{365}, a_{465} and a_{665} are the absorption coefficients at 250, 365, 465 and 665 nm. E2:E3 correlates inversely with DOM molecular size, while E4:E6 correlates inversely with DOM aromaticity and also with molecular size, O:C, C:N, carboxyl content and total acidity. E4:E6 can be used as general indicator of humification (Peuravuori and Pihlaja 1997).

Absorption slopes were computed for the entire wavelength range by using a non-linear estimation method based on the Levenberg-Marquardt algorithm for fitting the standard equation according to (Helms, Stubbins et al. 2008; Loiselle, Bracchini et al. 2009):

$$a_\lambda = a_0 * e^{-S(\lambda - \lambda_R)}$$

where a is the absorption coefficient at wavelength λ, λ_R is the lowest wavelength of the recorded spectrum (250nm) and a_0 – an indicator for CDOM concentration – is the absorption coefficient at the lowest recorded wavelength. The slope parameter S describes CDOM composition because it is correlated with the ratio of fulvic to humic acids and also shows correlation with the molecular weight of fulvic acids (Twardowski, Boss et al. 2004; Helms, Stubbins et al. 2008).
Also the spectral slope (SS) for a short wavelength region (275 – 295 nm) was computed and the slope ratio (S_R), which is the ratio of SS to a slope over a long wavelength region (350 – 400 nm).

$$S_R = \frac{S * (a_{275} - a_{295})}{S * (a_{350} - a_{400})}$$

SS and S_R are inversely correlated with molecular weight of DOM and have been identified as indicators of photodegradation (Helms, Stubbins et al. 2008).

CDOM can also be investigated by measuring fluorescence at specific excitation and emission wavelengths. Fluorescence-based excitation-emission matrices (EEMs) yielded indicators of recently produced and microbially derived DOM, terrestrially derived DOM and humification.

EEM signals due to water Raman scatter were eliminated from all spectra by subtracting a Milli-Q blank spectrum (Stedmon and Markager 2005).

Correction for the inner filter effect was done based on (McKnight, Boyer et al. 2001) using the following formulas:

$$A_{excit} = (\alpha * DOC) * 0.5$$

$$A_{emit} = (\beta * DOC) * 0.5$$

$$A_{total} = A_{excit} + A_{emit}$$

$$Correction\ factor = 10^{-A_{total}}$$

where A_{excit} is the absorbance of the excitation light at a given wavelength α, A_{emit} is the absorbance of the emitted light at a given wavelength β. The value 0.5 corresponds to half the pathlength of the 1 cm cuvette used. The resulting correction factor has to be applied to the fluorescence intensity measurement at the respective excitation and emission wavelength combination given by α and β. This is efficiently done by first computing a matrix of correction factors (of identical size to an EEM) which is then multiplied with the EEM to yield a corrected EEM. This removes the effect of absorption of incoming emission light and outgoing excitation light by the sample itself (McKnight, Boyer et al. 2001).

Furthermore, data from the Rayleigh scatter regions was deleted and a triangle of zeros was set below the Rayleigh band where emission wavelength > excitation wavelength (Stedmon and Bro 2008).

In corrected EEMs, individual peaks in predefined EEM-regions described in the literature were identified (Table 2) (Coble 1996). Further, a range of indices, ratios of fluorescence intensities at specific excitation/emission wavelength combinations, were computed from the corrected EEMs.

Table 2. This table shows specific excitation and emission wavelength of different peak types (Coble 1996).

Peak type	Fluorophore	Excitation (nm)	Emission (nm)
Humic like	A	237 – 260	400 – 500
Humic like	C	300 – 370	400 – 500
Protein like (Tyrosine)	B	225 – 237 275	309 – 321 310
Protein like (Tryptophan)	T1	225 – 237	340 – 381
Protein like (Tryptophan)		275	340

The peak ratio β:α – an indicator for autochthonous vs. allochthonous DOM sources – was calculated according to (Wilson and Xenopoulos 2008). This is the ratio of fluorescence intensity at an emission wavelength of 380 nm (β) to the maximum fluorescence intensity in the emission range of 420 – 435 nm (α). Both of them were measured at an excitation wavelength of 310 nm. The β-peak is regarded as a typically "microbial" peak related to autochthonous production, while α is regarded as indicating humic-like substances. β:α serves as a "freshness index" indicating the importance of recently produced DOM vs. more decomposed DOM components (Parlanti, Worz et al. 2000; Wilson and Xenopoulos 2008).

The fluorescence index was computed according to (McKnight, Boyer et al. 2001):

$$FI_{Ex\ 370nm} = \frac{Em_{450\ nm}}{Em_{500\ nm}}$$

This is the ratio of emission intensity at 450 nm to that at 500 nm obtained at an excitation wavelength of 370 nm. This index serves to distinguish sources of fulvic acids – it is higher for microbially derived, younger and autochthonous fulvic acids and lower for terrestrially derived, older and allochthonous fulvic acids (McKnight, Boyer et al. 2001).

Finally, the humification index (HI) defined as the area under the emission spectrum from 435 – 480 nm divided by the sum of the peak areas from 435 – 480 nm and 300 – 345 nm (Ohno 2002) was computed. There is a decreasing H:C ratio during humification which means a shift to more condensed molecules which show fluorescence at higher wavelength (De Haan and De Boer 1987). The corrected EEMs were also used for parallel factor analysis (PARAFAC), a multivariate three-way modeling technique that decomposes the fluorescence signal into individual components and provides estimates of the relative contribution of each component to the additively formed total signal (Bro 1997; Stedmon and Bro 2008). Each component identified by PARAFAC has a unique excitation and emission spectrum, a component can be a single fluorophore or a group of similar fluorophores. Once the number of components explaining the greatest variation in the data set are identified, the distribution of components can be calculated for each sample (Cory and McKnight 2005). Prior to PARAFAC, Rayleigh scatter regions with missing data were interpolated to speed up the modeling process (Bro, Bahram et al. 2006). PARAFAC was done using the DOMFluor toolbox for MATLAB 2007b following the manual by (Stedmon and Bro 2008). A maximum of 10 components was allowed, residual EEM plots were rigorously assessed and final models were validated by split-half validation and random initialization as recommended (Stedmon and Bro 2008).

2.6.2. Computation of pCO_2 and $epCO_2$

pCO_2, the partial pressure of CO_2 in the stream water (the pCO_2 in a hypothetical gas phase in equilibrium with the stream water), was determined via GC measurements.

If overpressure was not removed before GC pCO_2 values were corrected with a correction factor computed from

$$\frac{\dfrac{P_{lab} * V_{vial} * \ 10^{-3}}{R * T_{lab}}}{\dfrac{P_{field} * V_{vial} * \ 10^{-3}}{R * T_{field}}}$$

where P_{lab} is the atmospheric pressure in GC lab, computed from altitude in atm, V_{vial} stands for the volume of air filled into GC vials in ml and R is the gas constant (8,20575e[-05]). T_{lab} is the assumed temperature in the laboratory in K, P_{field} stands for the air pressure during measurement in stream in

atm. Original pCO$_2$ in sample water at experimental conditions was calculated using the Henry constant and atmospheric pressure during field work (Butler 1991).

Additionally, pCO$_2$ from DIC and pH was calculated with constants adjusted for temperature and ionic strength (Butler 1991; Stumm and Morgan 1996). First, dissolved and hydrated CO$_2$ (in M L^{-1}) has to be calculated:

$$[CO_2] = \frac{C_T}{1 + \frac{K_1'}{[H^+]} + \frac{K_1'K_2'}{[H^+]^2}}$$

where C_T is the total inorganic C in M L^{-1}, [H+] is the proton concentration computed from pH (M L^{-1}) as $10^{-pH}/\gamma$ with an activity coefficient γ computed as below. K_1' is the equilibrium constant for dissociation of H$_2$CO$_3$ (1st acidity constant of carbonic acid) and K_2' as the equilibrium constant for dissociation of HCO$_3$- (2nd acidity constant of carbonic acid).

The activity coefficient γ is computed from ionic strength I, i.e., the concentrations of all anions and cations determined empirically, using the Davies equation (Butler 1991), f is the mean molal activity coefficient and z is the ion charge.

$$\log \gamma = -0.5z^2 f(I)$$

Finally, pCO$_2$ was calculated with:

$$pCO_2 = \frac{[CO_2]}{K_H'} * 10^6$$

where K_H' is the Henry constant for CO$_2$ in M L^{-1} atm^{-1}.

For further calculations and statistical analysis data from GC analysis was used. To assess the potential of a stream as a source or sink for CO$_2$, excesspCO$_2$ (Ep$_{CO2}$ = pCO$_2$ WATER / pCO$_2$ ATMOSPHERE) was computed. Values of EpCO$_2$ > 1 and < 1 mean oversaturation and undersaturation of water with CO$_2$, respectively (Neal, House et al. 1998). The difference between CO$_2$ during day and night served as a proxy for metabolic activity and was calculated as pCO$_2$ night – pCO$_2$ day.

The CO$_2$-evasion rate (CO$_{2ev}$) was calculated with the formula:

$$CO_{2ev} = CO_{2str\ atm} * K_{CO_2} * \tau * Q$$

where $CO_{2 str\ atm}$ is the difference between CO_2 concentration in the stream and the atmosphere in $\mu mol\ L^{-1}$, K_{CO_2} is the gas transfer coefficient for CO_2 (min^{-1}), τ is the reach travel time in minutes and Q is the stream discharge in $L\ s^{-1}$. For area-specific CO_2 evasion the evasion rate was divided by the stream reach surface area (m^2) (Wallin, Öquist et al. 2011).

Alternatively, CO_2 evasion can be computed from (Raymond, Zappa et al. 2012):

$$CO_{2_{ev}} = CO_{2_{str\ atm}} * K_{CO_2} * d$$

where d is the depth in m.

2.6.3. Statistical analysis

Estimates of K_{CO_2} based on propane injections at selected stream sites were analysed as a function of the hydromorphological variables discharge, velocity, depth, width and slope using multivariate linear modelling and the Akaike Information Criterion (AIC) to select a suitable predictive model (Burnham and Anderson 2002; Quinn and Keough 2002). Rather than the mere identification of "significant" independents, the goal of IC-based model selection is the identification of a parsimonious model achieving high quality of fit (expressed in terms of a coefficient of determination) yet using the minimum necessary number of predictors. I assessed prediction quality of identified models using a "leave-one-out" cross-validation approach to evaluate the performance of the MLR-model. This procedure repeatedly rebuilds models leaving out data from one stream reach at a time and then uses this model to produce a single prediction for this left-out case which can be compared with its empirically determined counterpart (Hope, Dawson et al. 1995; Ripley 1996; Wallin, Öquist et al. 2011). The final model relating K_{CO_2} to hydromorphological variables was used to predict K_{CO_2} for the entire dataset of 105 sampling sites.

All statistical analyses were done with R 2.13.1 (R Development Core Team 2011) using the packages vegan, MASS and car.

3. Results

3.1. Hydromorphology

Table 3 shows mean, minimum and maximum discharge, width, depth, watersurface-slope (ws), streambed-slope (sb) and velocity across all sampled streams. Across the 105 sampling sites, discharge ranged from 1.64 to 5001.54 L s^{-1} with a mean of 364.91 L s^{-1}. Mean width was 5.31 m and ranged from 0.21 to 23 m. Depth ranged from 0.03 to 0.58 across the sampling sites with a mean of 0.20 m. The watersurface slope reached from -0.001 to -0.49 m m^{-1} with a mean slope of -0.04 m m^{-1}. Mean streambed slope across the sites was -0.03 m m^{-1} and ranged from -0.002 to -0.10 m m^{-1}. Velocity ranged from 0.001 to 1.67 m s^{-1} with a mean of 0.23 m s^{-1}.

Table 3. Hydromorphological values including mean, minimum (min), maximum (max) values and standard deviation (SD).

|	*mean*	*SD*	*min*	*max*
Discharge (L s^{-1})	364.91	± 883.08	1.64	5001.54
Width (m)	5.31	± 4.95	0.21	23
Depth (m)	0.20	± 0.12	0.03	0.58
Slope ws (m m^{-1})	-0.04	± 0.06	-0.001	-0.49
Slope sb (m m^{-1})	-0.03	± 0.02	-0.002	-0.10
Velocity (m s^{-1})	0.23	± 0.20	0.001	1.67

Across the entire network discharge shows a positive and highly significant correlation (Spearman, P<0.001) with Strahler stream order (Figure 6).
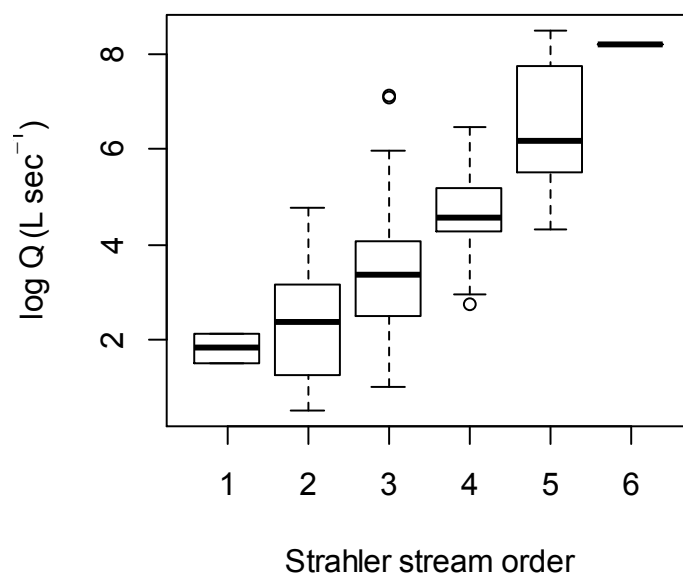
Figure 6. Discharge Q increases with stream size.

Hydraulic geometry analyses demonstrate positive correlations of width (w), depth (d) and velocity (v) with discharge (Q) shown in Figure 7.
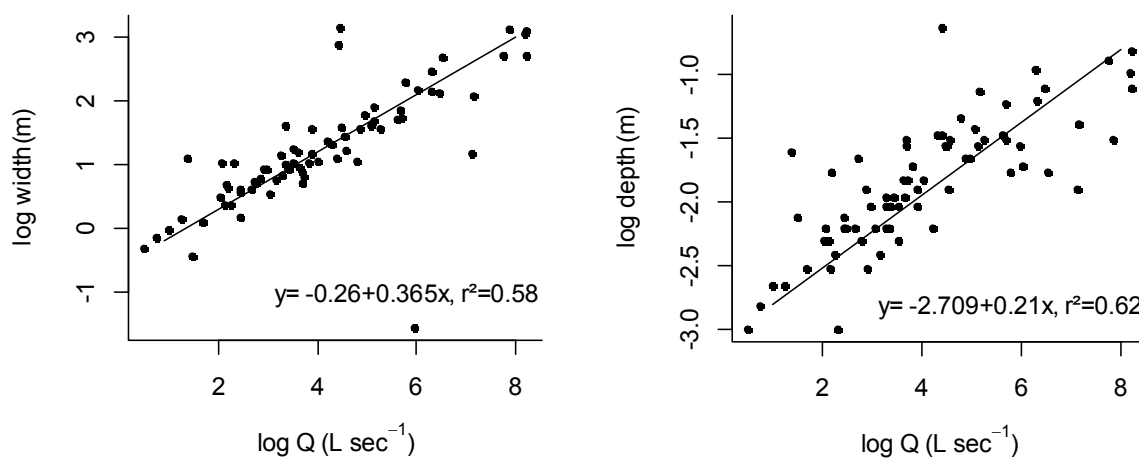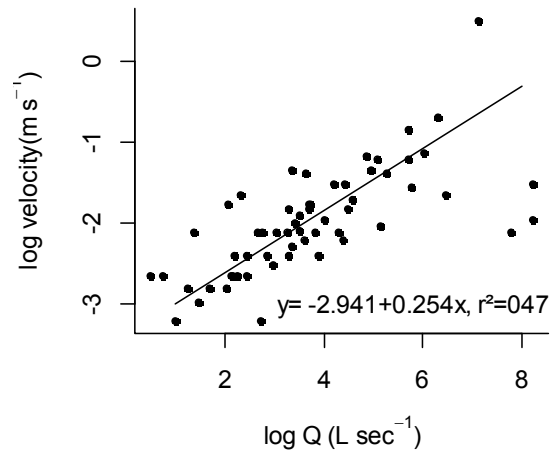
Figure 7. Hydraulic geometry after Leopold & Maddock (1953) where discharge Q is used as a proxy for stream size.

The hydraulic exponents are 0.37, 0.21 and 0.25 for width, depth and slope, respectively. For the coefficients -0.26, -2.709 and -2.941 were obtained.

In the sampled network water temperature ranges from -0.1 to 6.3°C with a mean of 2.45°C (Table 4) and increases significantly (Spearman, P<0.001) downstream.

Table 4. Mean water temperature and standard deviation in the sampled streams. Just one stream of 6th stream order was sampled.

order	mean (°C)	SD	min	max
1	1.13	0.81	0.2	1.7
2	1.91	1.16	0.0	3.75
3	2.36	1.49	-0.1	5.0
4	2.81	1.35	1.20	5.30
5	3.53	1.43	1.50	6.30
6	2.1	-	-	-

3.2. Gas exchange

The gas transfer coefficient of CO_2 (K_{CO2}) measured directly via propane injections in 23 stream reaches ranged from 0.0026 to 0.2472 min^{-1} with a mean of 0.0663 and a standard deviation of 0.0721 min^{-1}. Measured values are shown in Table 5, highest and lowest K_{CO2} were both observed in streams of 3rd stream order.

Table 5. K_{CO2} values across all sampled stream reaches with their identification number and stream order.

stream reach ID	stream order	K_{CO2} (min^{-1})	stream reach ID	stream order	K_{CO2} (min^{-1})
1	1	0.0539	13	3	0.0182
2	2	0.2473	14	3	0.0418
3	2	0.0026	15	3	0.0742
4	2	0.1280	16	4	0.0211
5	2	0.0279	17	4	0.0157
6	2	0.1294	18	4	0.0042
7	2	0.2390	19	4	0.0033
8	2	0.0407	20	4	0.0053
9	3	0.0566	21	4	0.0182
10	3	0.0315	22	4	0.0418
11	3	0.0998	23	4	0.0742
12	3	0.0855			

K_{CO2} in 1st stream order is 0.054 min^{-1}, mean K_{CO2} in 2nd stream order is 0.116 min^{-1}, 0.068 min^{-1} in 3rd stream order and streams of 4th stream order have a mean K_{CO2} of 0.023 min^{-1}. Literature values of K_{CO2} show similar scales (Table 6).

Table 6. Measured and literature based values of K_{CO2} in different stream orders.

order	mean K_{CO2} (min^{-1})	range (min^{-1})	mean K_{CO2} (min^{-1}) (Wallin, Öquist et al. 2011)	range (min^{-1}) (Wallin, Öquist et al. 2011)
1	0.054	–	0.028	0.013 – 0.076
2	0.116	0.003 – 0.247	0.022	0.012 – 0.057
3	0.068	0.032 – 0.100	0.020	0.012 – 0.042
4	0.023	0.003 – 0.074	1.017	0.011 – 0.034

On a double-logarithmic scale K_{CO2} was significantly related to discharge Q as the most powerful single predictor (Figure 8).
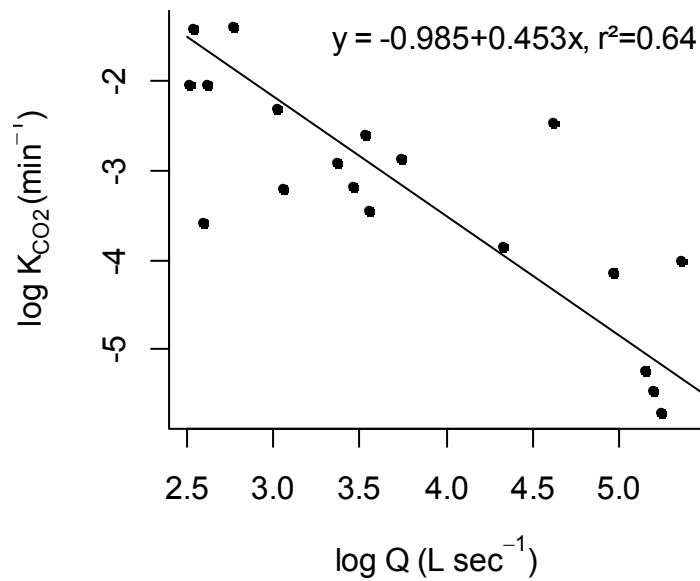
Figure 8. The gas transfer coefficient of CO_2 derived from continuous conservative gas tracer (propane) injection depends on discharge (P<0.001).

Predictive model selection based on the AIC resulted in the inclusion of slope, discharge and velocity (Table 7). The information criterion significantly includes discharge (P<0.01) and velocity (P<0.05) but also watersurface-slope.

**Table 7.** AIC suggested a model with the parameters watersurface-slope, discharge and velocity.

	Estimate	SD	P-value
$slope_{ws}$ (m m^{-1})	21.941	± 11.216	0.071
discharge (L s^{-1})	-0.731	± 0.196	0.002**
velocity (m s^{-1})	-0.036	± 0.015	0.036*

An even more complex model with the additional parameters depth and width (P>0.5) was rejected by the AIC (Table 8).

Table 8. The AIC shows that discharge, slope and velocity are the most reliable parameters.

|	Estimate	SD	P-value
depth (m)	2.939	± 5.331	0.594
width (m)	-0.172	± 0.179	0.350
$slope_{ws}$ (m m^{-1})	27.903	± 16.524	0.122
discharge (L s^{-1})	-0.734	± 0.309	0.039*
velocity (m s^{-1})	-0.035	± 0.023	0.163

Testing the models with a "leave one out" cross validation confirms significant predictive quality of both selected models (Figure 8).
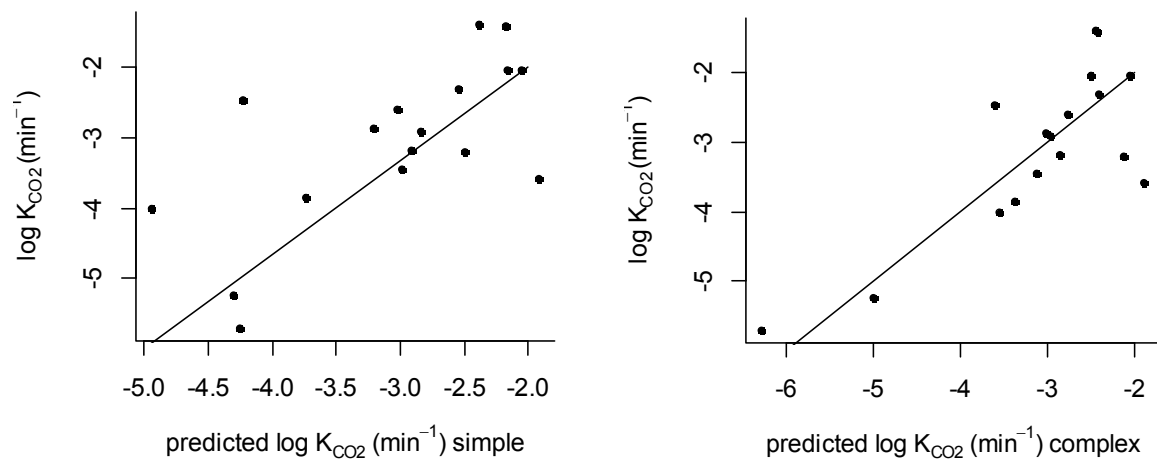
Figure 8. The cross-validation uses the model to predict K_{CO2} values and shows a positive correlation around the 1:1 line between measured and predicted K_{CO2}.
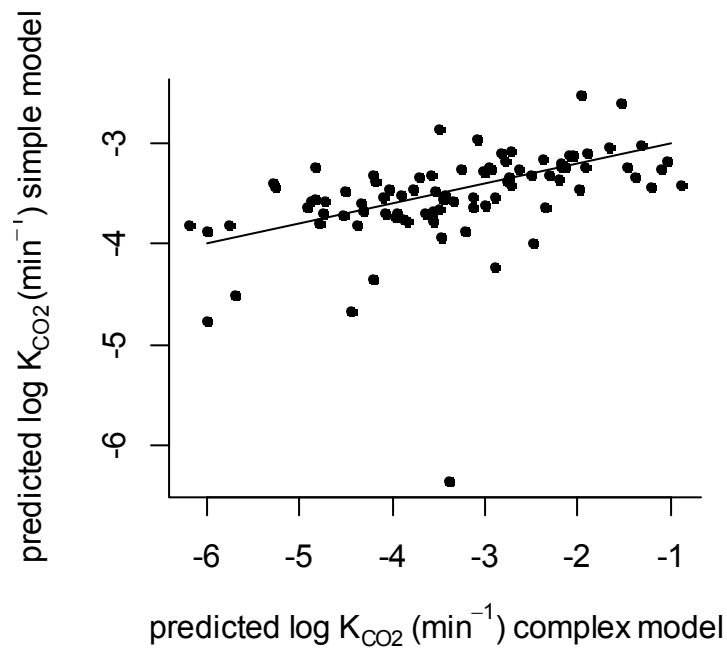
For the entire sampled network each model shows different results of predicted K_{CO2} values (Figure 9).

a)

b)
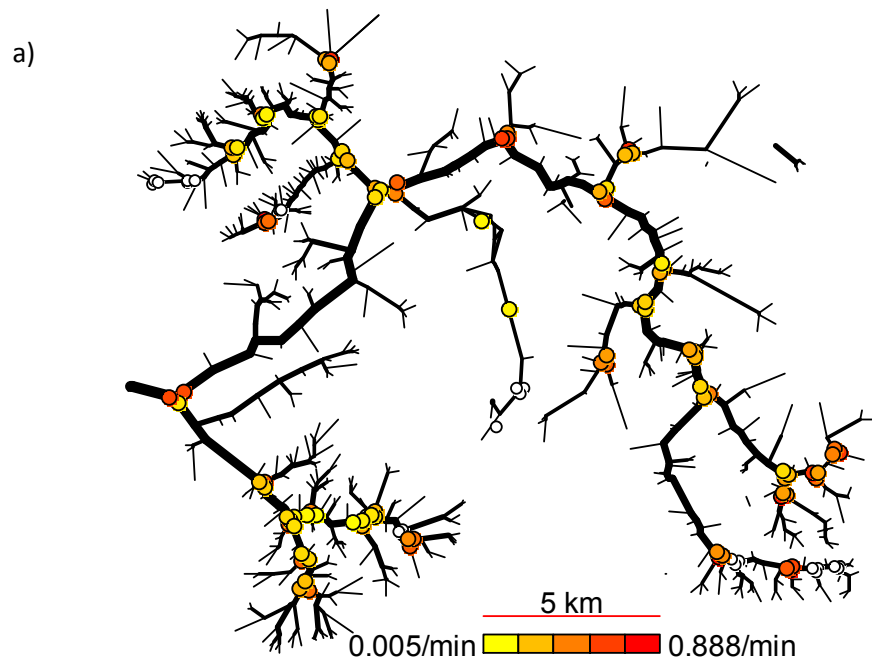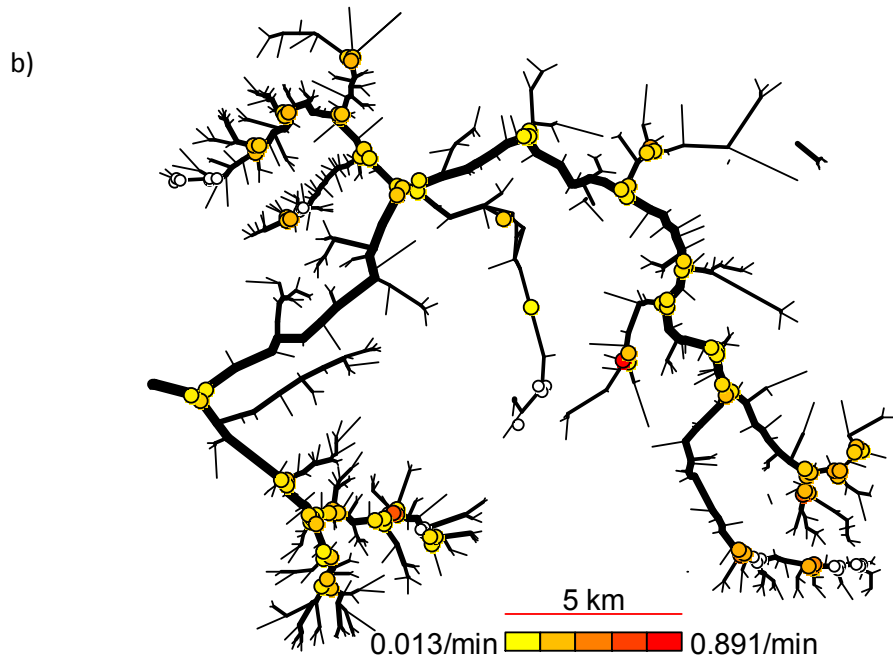
Figure 9. A graph of the entire network with K_{CO_2} values predicted from the simple model (a) and from the complex model (b). Yellow indicates low K_{CO_2} values.

Simple versus complex model shows different results (Figure 10).

Figure 10. K_{CO_2} values predicted with the complex model on the x-axis and K_{CO_2} predicted with the simple model on the y-axis.

3.3. CO_2

The partial pressure of CO_2 (pCO_2) measured by gas chromatography ranged from 262.58 to 1201.29 ppm with a mean of 508.83 ppm during the day. Mean pCO_2 at night was 595.10 ppm with a minimum of 343.22 and a maximum of 1395.86 ppm (Table 9).

Table 9. Mean, minimum and maximum pCO_2 in parts per million (ppm) and standard deviation during day and night, measured with gas chromatography.

sampling time	mean	SD	min	max
$pCO_2{}_{GC}$ day	508.83	± 206.37	262.58	1201.29
$pCO_2{}_{GC}$ night	595.10	± 280.87	343.22	1395.86

CO_2-concentrations (pCO_2) during the day correlate negatively but not significantly ($P>0.05$, $r^2=0.014$) with stream order ($P>0.05$, $r^2=0.04$) (Figure 11).
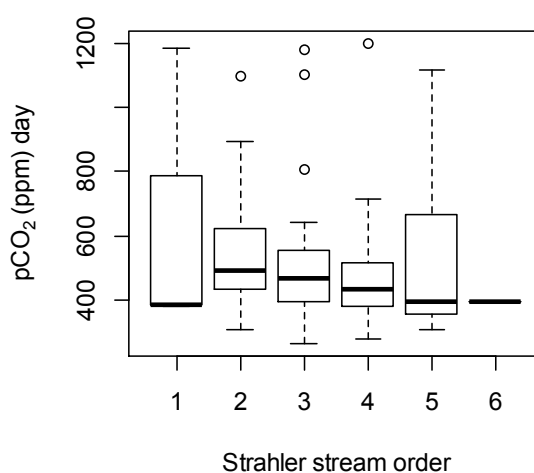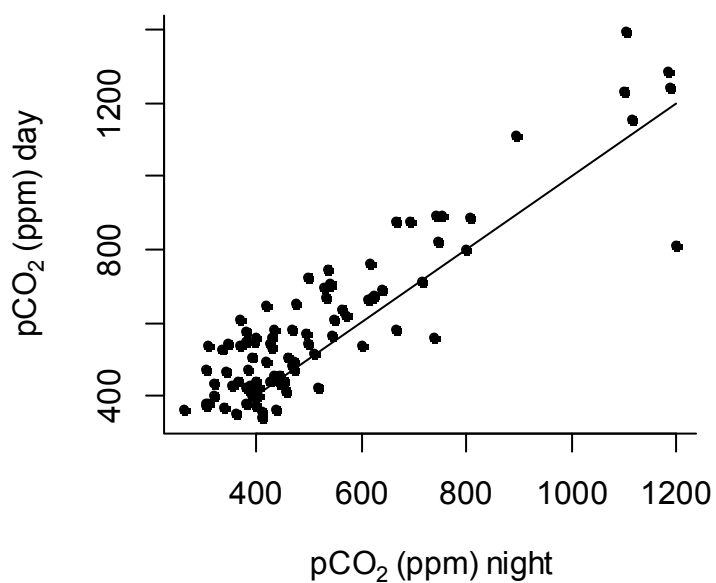

Figure 11. pCO_2 on the y-axes decreases with increasing stream size.

The same trend seems to be there in the night but becomes less clear (P>0.05, r^2=0.008) (Figure 12).
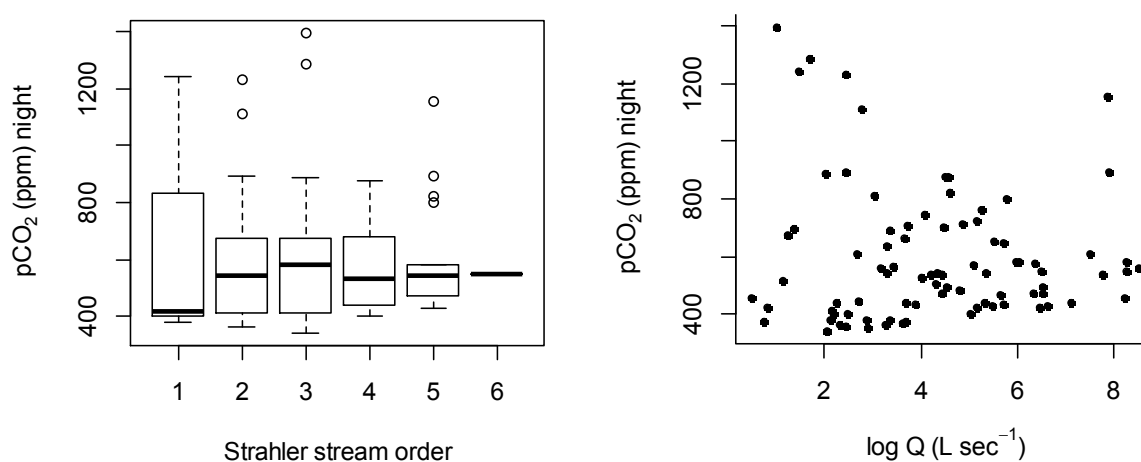

Figure 12. CO_2-concentrations also decrease slightly with stream size during the night.

Across all sampled streams CO_2 is higher during the night than during the day (Figure 13).

Figure 13. CO_2 values are slightly higher in the night.

Excess pCO_2 ($epCO_2$) ranges from 0.731 to 3.525 during the day and the mean of 1.414 indicates CO_2-supersaturation in many streams. Night $epCO_2$ ranges from 0.816 to 3.925, a mean of 1.637 shows even more supersaturation in the night. Generally smaller streams show a higher $epCO_2$ (Figure 14).
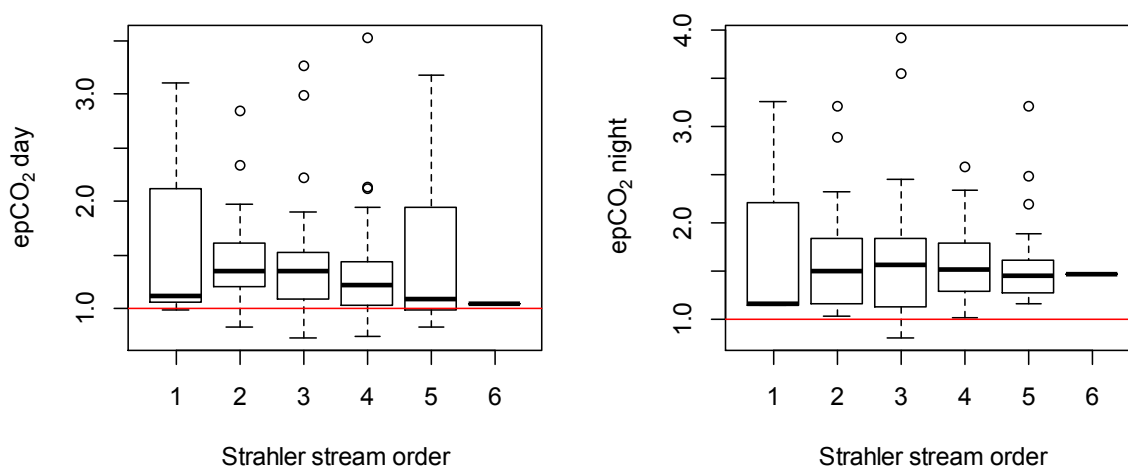
Figure 14. epCO2 during day (left) and during night (right). Values above the red line indicate CO_2-supersaturation.

The second method – pCO_2 calculated from DIC and pH – shows different results. Mean pCO_2 is 677.56 and ranges from 245.998 to 1445.84 during the day. During the night pCO_2 ranges from 340.64 to 1780.74 with mean pCO_2 of 595.10 (Table 10).

Table 10. The table shows pCO_2 in ppm calculated from dissolved inorganic carbon (DIC) and pH-values including standard deviation, mean, minimum and maximum pCO_2 during day and night.

sampling time	mean	SD	min	max
$pCO_{2\ DIC/pH}$ day	677.56	± 256.62	245.998	1445.84
$pCO_{2\ DIC/pH}$ night	340.64	± 398.99	340.64	1780.74

CO_2-concentrations (pCO_2) during day and night do not really show a clear negative correlation with stream order ($P>0.05$, $r^2=0.0003$ for day, $P>0.05$, $r^2=0.004$ for night) (Figure 15).
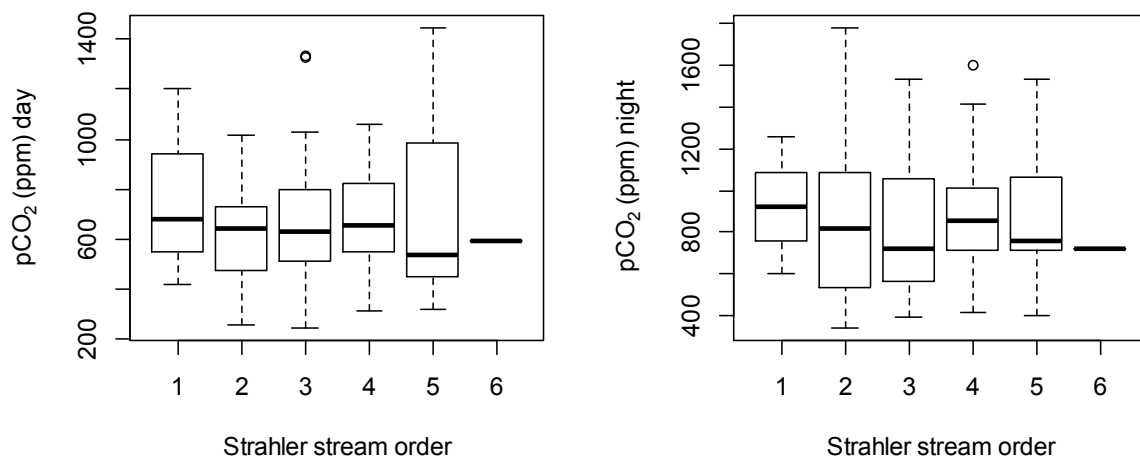
Figure 15. pCO_2 during the day (left) and during the night (right) calculated from DIC and pH as a function of stream order (indicating stream size) does not show a clear negative trend.

If calculated from DIC and pH, pCO_2 shows more variation during day and night (Figure 16).
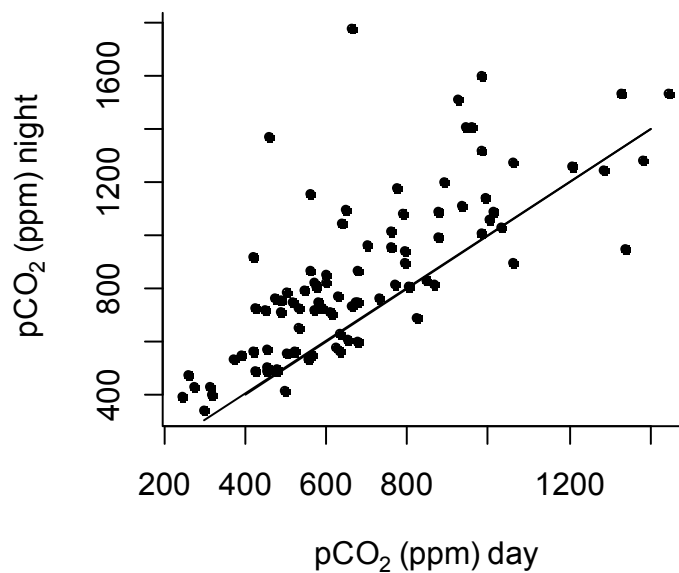
Figure 16. pCO_2-values vary more if calculated from DIC and pH. CO_2-concentrations are higher during the night than during the day.

Comparing both methods shows a clear difference in CO_2-concentrations derived from direct measurement via GC or indirect measurement via DIC/pH. While both methods show lower CO_2-concentrations during the day. the DIC/pH-method tends to result in higher CO_2-concentrations (Figure 17).
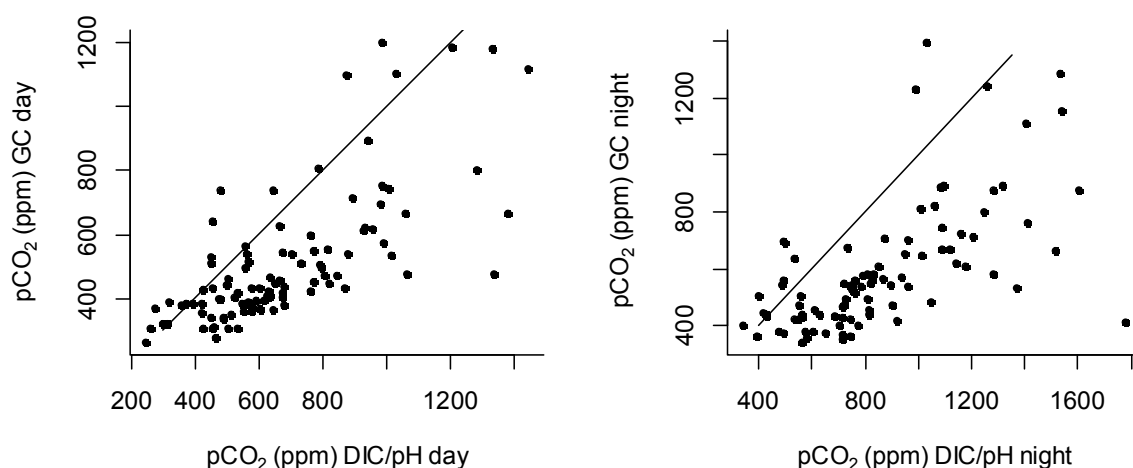

Figure 17. There is a clear difference between CO_2 calculated from DIC/pH on the x-axis compared with CO_2 from GC on the y-axis. The left graph shows pCO_2 during day while pCO_2 in the night is shown on the right.

3.4. CO_2-evasion

Area-specific CO_2-evasion rate predicted for the whole network (Table 11) and based on K_{CO2} predicted from the simple model ranges from 0.0.0143 to 338.666 µmol sec^{-1} m^{-2} during the day, with a mean evasion-rate of 11.490 ± 35.791 µmol sec^{-1} m^{-2}. Evasion rate in the night ranges from 0.017 to 732.294 µmol sec^{-1} m^{-2} with a mean of 23.123 ± 75.8918 µmol sec^{-1} m^{-2}. Prediction of K_{CO2} with the complex model results in evasion rates from 0.019 to 380.828 µmol sec^{-1} m^{-2} during the day with a mean of 10.245 ± 38.498 µmol sec^{-1} m^{-2} . Mean evasion rate during the night is then 20.497 ± 75.293 µmol sec^{-1} m^{-2} and ranges from 0.016 to 735.176 µmol sec^{-1} m^{-2}.

Table 11. Mean evasion-rate in $\mu mol\ sec^{-1}\ m^{-2}$ is higher during the night than during the day and varies between prediction with simple and complex model.

Model	day/night	mean CO_2 evasion-rate ($\mu mol\ sec^{-1}\ m^{-2}$)
simple	day	11.490 ± 35.791
simple	night	23.123 ± 75.8918
complex	day	10.245 ± 38.498
complex	night	20.497 ± 75.293

CO_2-evasion rate predicted with the complex model (day and night data included) show a clear negative downstream trend, even though the correlation is not significant ($P>0.05$) (Figure 18).
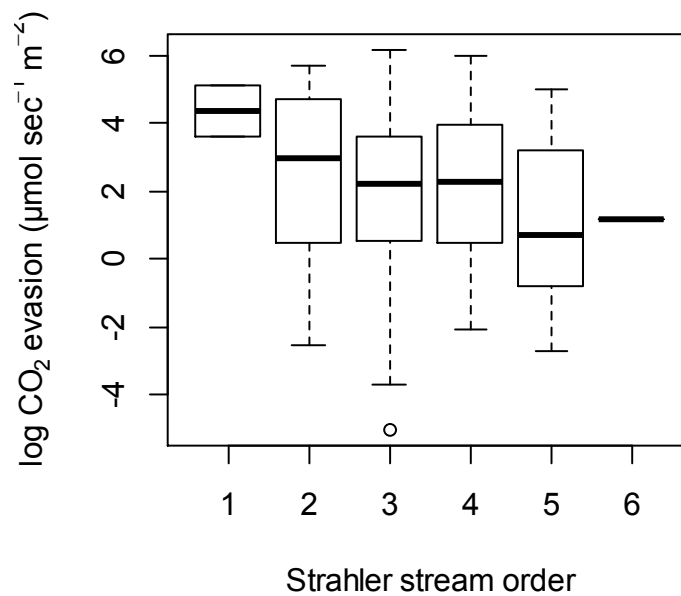
Figure 18. Headwater streams show the highest mean evasion rates, 5th order streams show the lowest evasion rates.

3.5. pH and DIC

Water-pH ranged from 8.030 to 8.779 with a mean of 8.375. pH-values seem to increase downstream (Table 12).

Table 12. pH increases with increasing stream order.

order	mean	SD	min	max
1	8.296	0.056	8.254	8.360
2	8.368	0.163	8.030	8.601
3	8.384	0.147	8.089	8.779
4	8.384	0.140	8.206	8.746
5	8.366	0.173	8.044	8.661
6	8.405	–	–	–

DIC ranges from 22.99 to 58.42 ppm during the day with a mean of 40.91 ± 6.73 ppm. Mean DIC concentration during the night is 41.22 ± 14.35 ppm and ranges from 22.75 to 54.39 ppm (Table 13).

Table 13. Mean, minimum and maximum DIC concentrations during day and night including standard deviation.

	mean	SD	min	max
DIC day	40.91	± 6.73	22.99	58.42
DIC night	41.22	± 14.35	22.75	54.39

3.6. Ions

The following ion concentrations were measured (Table 14).

Table 14. Mean, minimum and maximum ion concentrations with standard deviation in mg L^{-1}.

Ion	mean	SD	min	max
Sodium	1.4	± 1.6	0.2	6.9
Potassium	0.3	± 0.3	0.0	1.3
Calcium	46.0	± 8.5	32.0	67.5
Magnesium	16.7	± 6.3	2.3	25.8
Chloride	1.6	± 1.8	0.3	7.9
Nitrate	4.4	± 0.9	1.8	6.9
Sulfate	4.8	± 4.6	1.5	38.1

A PCA (Principal Component Analysis) shows different ion concentrations in each stream, and low stream orders tend to differ more than higher orders (Figure 19).
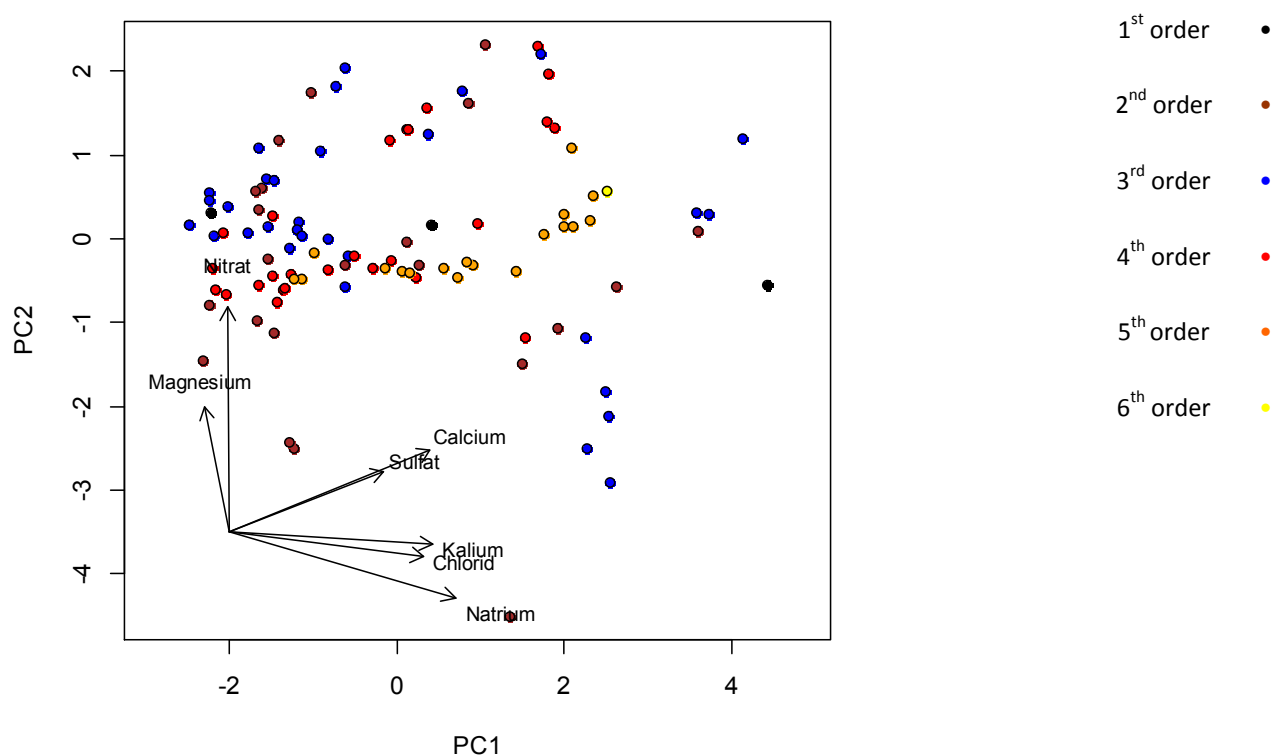
Figure 19. Low stream orders differ more in ion composition than higher stream orders, the latter ones are centrally positioned.

3.7. Dissolved organic carbon

DOC during day-sampling ranged from 0.511 to 2.553 ppm with a mean of 1.359 ppm ± 0.437 ppm. Median DOC in the night is 1.352 ppm ± 0.589 ppm, the concentrations vary from 0.563 to 2.535 ppm. Median DOC-concentration during night and day is 1.356 ppm ± 0.435 ppm and ranges from 0.537 to 2.544 ppm. DOC does not significantly correlate with stream order across the entire sampled network (Spearman, P>0.05) (Figure 20).
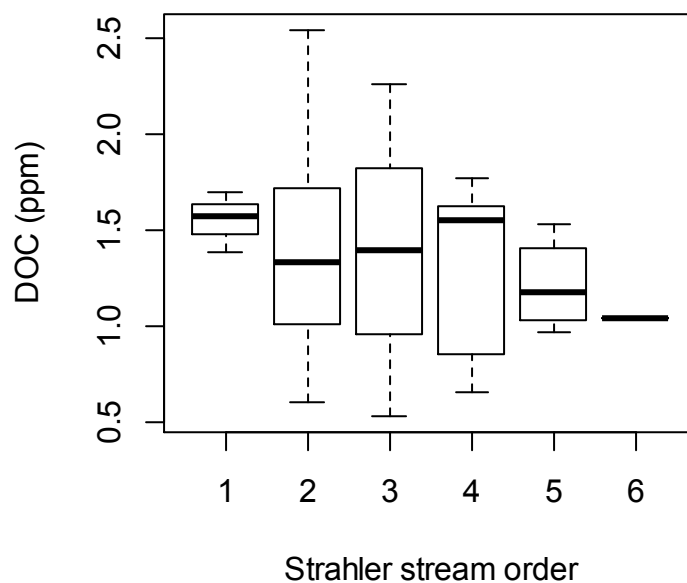
Figure 20. DOC-concentrations (in ppm) decrease with increasing stream order.

The absorbance coefficient at a wavelength of 254 nm ranges from 2.602 to 19.503 with a mean of 8.697 and does not significantly ($P>0.05$) correlate with stream size. Therefore the mean specific UV-absorbance at a wavelength of 254 nm decreases significantly downstream ($P<0.05$), $SUVA_{254}$ ranges from 4.286 to 7.777 with a mean of 6.225 (Figure 21).

The Humification Index (HIX) ranges from 0.255 to 0.401 with a mean of 0.347 and also decreases significantly (Spearman, P<0.05) with increasing stream size (Figure 22).
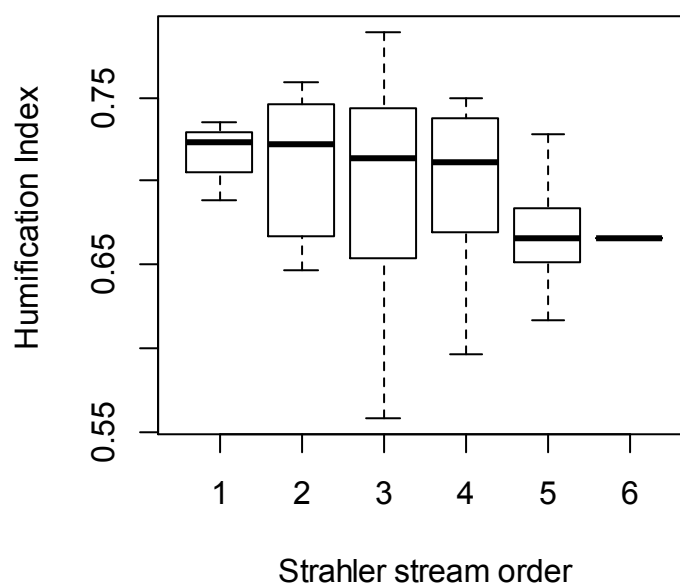
Figure 22. Also the Humification Index correlates significantly with stream order.

A PCA with DOC data (including DOC concentration, stream order, E2:E3, E4:E6, Fluorescence Index FIX, Humification Index HIX, absorbance coefficient at 254 nm, SUVA$_{254}$ and β:α) shows clearly separated stream orders (Figure 23).
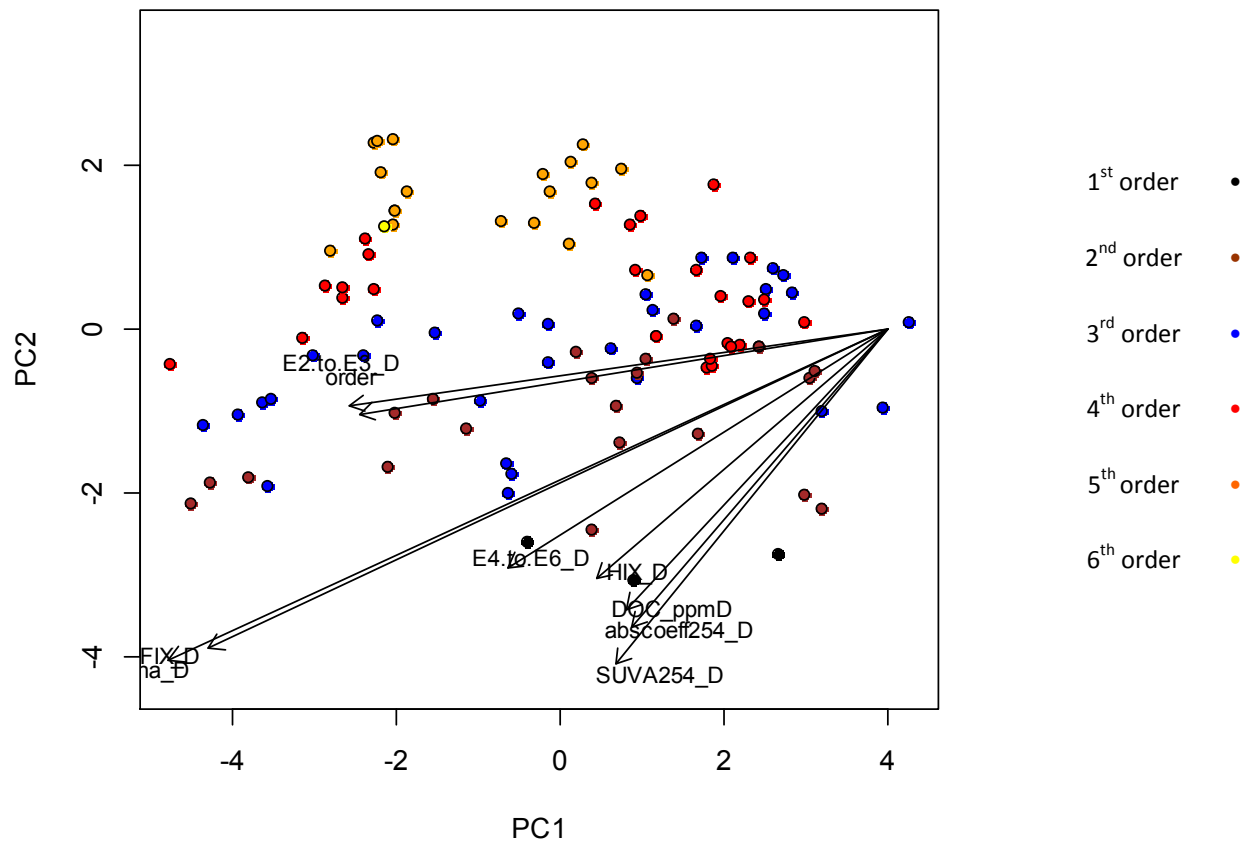
Figure 23. The PCA shows clear distribution of stream order and more differentiation of DOM among streams of lower orders.

4. Discussion

4.1. Hydromorphology

The relationships between depth, width, velocity and discharge are similar for all river systems even though they differ in physiographic conditions. Increasing discharge is related to increasing depth, width and velocity with simple power functions. It is not surprising that this study also shows the relationships between these hydrological parameters. The hydraulic exponents in this study were 0.37, 0.21 and 0.25 for width, depth and slope, respectively, and sum up to 0.83 (≤1.0). Also the coefficients -0.26, -2.709 and -2.941 are consistent to (Leopold and Maddock 1953).

A comparison with the data from (Raymond, Zappa et al. 2012) shows a difference in hydraulic parameters (Table 15).

Table 15. A hydraulic geometry comparison of the two datasets.

source	width	depth	velocity
own study	y=-0.26+0.365x	y=-2.709+0.210x	y=-2.941+0.254x
Raymond, 2012	y=2.56+0.423x	y=-0.895+0.294x	y=-1.64+0.285x

The variation between the two studies is probably caused by the difference of the investigated fluvial networks. Streams and rivers in and around Lunz are very steep, furthermore my study contains a lot of small rivers. While Raymond et al. used a very large dataset originating from measurements made by the U.S. Geological Survey, where the average of the streams/rivers are not marked by an alpine character as the ones used in my own study.

4.2. Gas exchange

The gas transfer coefficient (K_{CO_2}) values ranging from 0.0001 to 0.339 min^{-1} are similar with those described in the literature (Melching and Flores 1999; Wallin, Öquist et al. 2011), but the number of K_{CO_2} studies is still limited. Highest K_{CO_2} values were observed in small streams characterized by steeper and shallow stream reaches where more CO_2 can evade to the atmosphere and as already described in literature, discharge is a key variable to explain K_{CO_2} variability (Hope, Palmer et al. 2001). This study is a basis to define relationships between K_{CO_2} and hydrological parameters like discharge and/or slope and velocity. The simple model, which predicts K_{CO_2} based on discharge, is a relatively rapid and simple method to get an idea of K_{CO_2} variability across an entire network. This can

be confirmed with a good performance when testing the model with a leave-one-out cross-validation. Also the more complex model could be a good base to estimate K_{CO2} for river networks as demonstrated by the same cross-validation.

4.3. CO_2 and CO_2-evasion

The big difference between the two used methods to determine pCO_2 in water demonstrates that a more reliable method to measure CO_2-concentrations needs to be found. As the simpler and faster method DIC/pH results in less useful data which seems to overestimate CO_2-concentrations. Measurements with GC should thus be preferred. Recent studies on pCO_2 use GC (Wallin, Öquist et al. 2011), calculate pCO_2 from pH, alkalinity, cations, DOC/TOC and temperature (Humborg, Morth et al. 2010) or use an infrared CO_2 analyzer (Zeng and Masiello 2010).

Measured CO_2-concentrations differ during day and night, the mean pCO_2 during the day is 508.83 ppm and it is 595.10 ppm in the night. Light allows photosynthetic activity during the day, and as there is no photosynthesis in the night and respiratory activity is high, CO_2 increases.

Streams receive large amounts of terrestrial C such as roots, litter or soil organic carbon. Especially low-order, narrow rivers receive more loading of terrestrial C because of more canopy cover. Due to their small size they can be regarded as more interdependent with their surrounding landscape (Vannote, Minshall et al. 1980; Zeng and Masiello 2010). Higher C loads imply increased potential for metabolism and thus high pCO_2. As a consequence, there is a downstream gradient of pCO_2, and as it decreases with stream order, it suggests that there is less metabolic activity in larger streams.

Most streams and rivers are supersaturated with CO_2 relative to the atmosphere indicating a constant flux of CO_2 due to vertical evasion (Cole and Caraco 2001). Nearly all sampled streams have $epCO_2 > 1$ indicating supersaturation, while in this study small streams are more supersaturated than larger streams. Literature shows that small streams are likely to be more saturated than larger ones (Finlay 2003). This difference can be explained with an already supersaturated groundwater inflow in headwater streams.

My study pictures that small streams have a higher CO_2-evasion rate than larger streams. The reason is more surface turbulence in small streams which affects the aquatic boundary layer leading to a greater gas exchange potential at the water-air interface (Macintyre, Wanninkhof et al. 1995). Also, respiration in organic-rich soils leads to high concentration of dissolved gases in soil water, which constitutes a significant input of CO_2-supersaturated water into headwaters. The mass flow of dissolved gases into the lower part of the catchment decreases downstream as more inorganic carbon converts to bicarbonate as CO_2 degasses and the pH of the stream increases (Hope, Palmer

et al. 2001). Finally, the study shows that CO_2-concentrations and CO_2-evasion rates vary significantly along a stream network indicating the importance of catchment characteristics such as topography or hydrology.

4.4. pH and DIC

The DIC concentration seems to be lower in streams with higher discharge, which is probably associated with carbonate dissolution. When carbonate is dissolved by soil-CO_2, CO_2 is sequestrated as bicarbonate, this is why carbonate dissolution can be regarded as a sink of atmospheric CO_2 (Zeng and Masiello 2010). Higher DIC – as well as CO_2 – concentrations in smaller streams get lost along the stream reaches through evasion and this evasion rate is higher than the input rate of DIC from groundwater inputs along the stream (Wallin, Buffam et al. 2010). This is why streams with higher stream order have a lower DIC concentration.

4.5. Ions

With 46.0 mg L^{-1} and 16.7 mg L^{-1} Calcium and Magnesium formed the most common ionic species in the stream network, which is a simple consequence of the predominantly carbonaceous geology of the catchment. As the PCA shows, headwater streams vary more in ion composition than larger streams. Streams with higher stream orders are thoroughly mixed and receive ions from various inflows, whereas headwater streams have different sources with varying ion composition.

4.6. Dissolved organic carbon

As shown in this study, DOC decreases downstream. Headwaters receive most of the terrestrial DOC, this results from their drainage length, density and because they interdigitate more within the landscape. The DOC is then continuously metabolized along the fluvial network via photolysis, shifts in microbial community composition and DOC aggregation, for instance (Battin, Kaplan et al. 2008).

The specific UV absorbance at a wavelength of 254 nm ($SUVA_{254}$) is an indicator for the dissolved aromatic carbon content and the humic fraction of the DOC (Weishaar, Aiken et al. 2003). The Humification Index (HIX) – determining the degree of humification – measures the condensed (aromatic) fraction of the DOC (Zsolnay, Baigar et al. 1999). In my study both parameters decrease significantly downstream, indicating that smaller streams are more affected by the surrounding landscape.

Zusammenfassung

Der globale Kohlenstoff-Zyklus rückt immer mehr in das Interesse der Wissenschaft. Mehrere Studien haben bereits bestätigt, dass Fließgewässer und Seen einen großen Teil zu globalen Kohlenstoff-Flüssen beitragen. Es gibt schon einige Daten zu CO_2-Ausgasung von einzelnen Seen oder Flüssen, aber über den CO_2-Ausstoß von ganzen Fließgewässer-Netzwerken ist noch sehr wenig bekannt. In dieser Studie habe ich die Kohlendioxid-Ausgasung eines alpinen Flussnetzwerkes (Ybbs, Niederösterreich) gemessen. Die 105 beprobten Flüsse reichten von der ersten bis zur sechsten Flussordnung, das gesamte Einzugsgebiet hat eine Fläche von ca. 400 km². In allen Flüssen wurden Durchfluss, Gefälle, Tiefe und Breite gemessen. Kohlendioxid-Konzentrationen wurden mittels pCO_2 (Partialdruck von CO_2) gemessen. Hierbei stellte sich heraus, dass das ganze Flussnetzwerk CO_2-übersättigt ist, außerdem gibt es klare Unterschiede zwischen Tag und Nacht. Um den CO_2-Transferkoeffizienten zu bestimmen wurden bei 20 ausgewählten Flüssen Propan-Injektionen durchgeführt. Der Koeffizient zeigt eine positive Korrelation mit dem Durchfluss, dieser hydrologische Parameter wurde somit auch verwendet um den Transferkoeffizienten der übrigen 85 Flüsse vorherzusagen. Auch optische Parameter von gelöstem organischen Kohlenstoff wurden gemessen, hiermit konnte die räumliche Variation von CO_2 erklärt werden.

Curriculum Vitae

Name: Sabrina Hengsberger

Geburtsdatum und -ort: 06.07.1986 in Hallein, Salzburg

Staatsbürgerschaft: Österreich

Schulbildung: 1992 – 1996 VS Neue Heimat Bischofshofen

1996 – 2005 PG St. Rupert Bischofshofen

2005 – 2009 Bachelorstudium Ökologie/Biodiversität Uni Salzburg

Seit 2010 Masterstudium Ökologie Uni Wien

Wissenschaftliche Berufserfahrung:

2007 – Datenerfassung für die Bachelorarbeit

      in der Tropenstation La Gamba, Costa Rica

2012 – Projektmitarbeit („Priming" – DeLi) Uni Wien

Fremdsprachen: Englisch, Spanisch, Grundkenntnisse in Französisch und Italienisch

References

Aiken, G. and J. Leenheer (1993). "Isolation and Chemical Characterization of Dissolved and Colloidal Organic Matter." Chemistry and Ecology **8**(3): 135-151.

Amon, R. M. W. and R. Benner (1996). "Bacterial utilization of different size classes of dissolved organic matter." Limnology and Oceanography **41**(1): 41-51.

Aufdenkampe, A. K., E. Mayorga, et al. (2011). "Riverine coupling of biogeochemical cycles between land, oceans, and atmosphere." Frontiers in Ecology and the Environment **9**(1): 53-60.

Barnes, R. T. and P. A. Raymond (2009). "The contribution of agricultural and urban activities to inorganic carbon fluxes within temperate watersheds." Chemical Geology **266**(3-4): 327-336.

Battin, T. J., L. A. Kaplan, et al. (2008). "Biophysical controls on organic carbon fluxes in fluvial networks." Nature Geoscience **1**: 95-100.

Battin, T. J., S. Luyssaert, et al. (2009). "The boundless carbon cycle." Nature Geoscience **2**: 598-600.

Bro, R. (1997). "Parafac. Tutorial and Applications." Chemometrics and Intelligent Laboratory Systems **38**(2): 149-171.

Bro, R., M. Bahram, et al. (2006). "Handling of Rayleigh and Raman scatter for PARAFAC modeling of fluorescence data using interpolation." Journal of Chemometrics **20**(3-4): 99-105.

Brown, B. L., C. M. Swan, et al. (2011). "Metacommunity theory as a multispecies, multiscale framework for studying the influence of river network structure on riverine communities and ecosystems." Journal of the North American Benthological Society **30**(1): 310-327.

Burnham, K. P. and D. R. Anderson (2002). Model Selection and Multimodel Interference: A Practical Information-Theoretic Approach. New York, U.S.A., Springer.

Butler, J. N. (1991). Carbon dioxide equilibria. Chelsea, Michigan, USA, Lewis Publishers.

Camper, A. K. (2004). "Involvement of humic substances in regrowth." International Journal of Food Microbiology **92**(3): 355-364.

Coble, P. G. (1996). "Characterization of marine and terrestrial DOM in seawater using excitation emission matrix spectroscopy." Marine Chemistry **51**(4): 325-346.

Cole, A. C. and N. Caraco (2001). "Carbon in catchments: connecting terrestrial carbon losses with aquatic metabolism." Marine & Freshwater Research **52**: 101-110.

Cole, J. J. (2007). "Plumbing the global carbon cycle: Integrating inland waters into the terrestrial carbon budget." Ecosystems **10**(1): 172-185.

Cory, R. M. and D. M. McKnight (2005). "Fluorescence spectroscopy reveals ubiquitous presence of oxidized and reduced quinones in dissolved organic matter." Environmental Science & Technology **39**(21): 8142-8149.

Cummins, K. W. (1974). "Stream ecosystem structure and function." BioScience **24**: 631-641.

De Haan, H. and T. De Boer (1987). "Applicability of light absorbance and fluorescence as measures of concentration and molecular size of dissolved organic carbon in humic lake Tjeukemeer." Water Research **21**(6): 731-734.

Del Vecchio, R. and N. V. Blough (2004). "On the origin of the optical properties of humic substances." Environmental Science & Technology **38**(14): 3885-3891.

Demars, B. O. L., J. R. Manson, et al. (2011). "Temperature and the metabolic balance of streams." Freshwater Biology **56**(6): 1106-1121.

Fellmann, J. B., E. Hood, et al. (2010). "Fluorescence spectroscopy opens new windows into dissolved organic matter dynamics in freshwater ecosystems: A review." Limnology and Oceanography **55**(6): 2452-2462.

Finlay, J. C. (2003). "Controls of streamwater dissolved inorganic carbon dynamics in a forested watershed." Biogeochemistry **62**(3): 231-252.

Füreder, L. and M. Pöckl (2007). Ecological traits of aquatic NIS invading Austrian fresh waters. Biological invaders in inland waters: Profiles, distribution, and threats. F. Gherardi. ??, Springer**:** 233-257.

Genereux, D. P. and H. F. Hemond (1992). "Determination of Gas-Exchange Rate Constants for a Small Stream on Walker Branch Watershed, Tennessee." Water Resources Research **28**(9): 2365-2374.

Gordon, N. D., T. A. McMahon, et al. (2004). Stream Hydrology, an Introduction for Ecologists. Chichester, England, John Wiley & Sons Ltd.

Grant, E. H. C., W. H. Lowe, et al. (2007). "Living in the branches: population dynamics and ecological processes in dendritic networks." Ecology Letters **10**(2): 165-175.

Harvey, C. J. and B. J. Peterson (1997). "Organic matter dynamics in the Kuparuk River, a tundra river in Alaska, USA." Journal of the North American Benthological Society 16: 18-23.

Helms, J. R., A. Stubbins, et al. (2008). "Absorption spectral slopes and slope ratios as indicators of molecular weight, source, and photobleaching of chromophoric dissolved organic matter." Limnology and Oceanography 53(3): 955-969.

Hertkorn, N., M. Frommberger, et al. (2008). "Natural organic matter and the event horizon of mass spectrometry." Analytical Chemistry 80(23): 8908-8919.

Hillebrand, H., E. T. Borer, et al. (2009). "Herbivore metabolism and stoichiometry each constrain herbivory at different organizational scales across ecosystems." Ecology Letters 12(6): 516-527.

Hope, D., J. J. C. Dawson, et al. (1995). "A Method for Measuring Free CO_2 in Upland Streamwater Using Headspace Analysis." Journal of Hydrology 166(1-2): 1-14.

Hope, D., S. M. Palmer, et al. (2001). "Carbon dioxide and methane evasion from a temperate peatland stream." Limnology and Oceanography 46(4): 847-857.

Humborg, C., C. M. Morth, et al. (2010). "$CO(2)$ supersaturation along the aquatic conduit in Swedish watersheds as constrained by terrestrial respiration, aquatic respiration and weathering." Global Change Biology 16(7): 1966-1978.

Johnson, M. S., M. F. Billett, et al. (2010). "Direct and continuous measurement of dissolved carbon dioxide in freshwater aquatic systems-method and applications." Ecohydrology 3(1): 68-78.

Jones, J. B. and P. J. Mulholland (1998). "Carbon dioxide variation in a hardwood forest stream: An integrative measure of whole catchment soil respiration." Ecosystems 1(2): 183-196.

Jones, R. I., J. Grey, et al. (1998). "An assessment, using stable isotopes, of the importance of allochthonous organic carbon sources to the pelagic food web in Loch Ness." Proceedings of the Royal Society London B 265: 105-111.

Kaplan, L. A. and D. J. Newbold (2003). The role of monomers in stream ecosystem metabolism. Aquatic ecosystems: Interactivity of dissolved organic matter. S. E. G. Findlay and R. L. Sinsabaugh. San Diego, California, Academic Press: 97-119.

Kim, S., L. A. Kaplan, et al. (2006). "Biodegradable dissolved organic matter in a temperate and a tropical stream determined from ultra-high resolution mass spectrometry." Limnology and Oceanography 51(2): 1054-1063.

Kim, S., A. J. Simpson, et al. (2003). "High resolution electrospray ionization mass spectrometry and 2D solution NMR for the analysis of DOM extracted by C-18 solid phase disk." Organic Geochemistry **34**(9): 1325-1335.

Lamberti, G. A. and A. D. Steinman (1997). "A comparison of primary production in stream ecosystems." Journal of the North American Benthological Society **16**(1): 95-104.

Leopold, L. B. and T. Maddock (1953). "The Hydraulic Geometry of Stream Channes and some Physiographic Implications." U.S. Government Printing Office **57**.

Loiselle, S. A., L. Bracchini, et al. (2009). "Optical characterization of chromophoric dissolved organic matter using wavelength distribution of absorption spectral slopes." Limnology and Oceanography **54**(2): 590-597.

Loreau, M., N. Mouquet, et al. (2003). "Biodiversity as spatial insurance in heterogeneous landscapes." Proceedings of the National Academy of Sciences, USA **100**(22): 12765-12770.

Lyon, D. R. and S. E. Ziegler (2009). "Carbon cycling within epilithic biofilm communities across a nutrient gradient of headwater streams." Limnology and Oceanography **54**(2): 439-449.

Macintyre, S. R., R. Wanninkhof, et al., Eds. (1995). Trace gas exchange across the air-water interface in freshwater and coastal marine environments. Biogenic trace gases: Measuring emissions for soil and water. Oxford, Blackwell Science.

Marzolf, E. R., P. J. Mulholland, et al. (1994). "Improvements to the diurnal upstream-downstream dissolved oxygen change technique for determining whole-stream metabolism in small streams." Canadian Journal of Fisheries and Aquatic Sciences **51**: 1591-1599.

McKnight, D. M., E. W. Boyer, et al. (2001). "Spectrofluorometric characterization of dissolved organic matter for indication of precursor organic material and aromaticity." Limnology and Oceanography **46**(1): 38-48.

Melching, C. S. and H. E. Flores (1999). "Reaeration equations derived from US geological survey database." Journal of Environmental Engineering-Asce **125**(5): 407-414.

Metzger and Dobbins (1967). "Role of fluid properties in gas transfer." Environmental Science & Technology **1**(1): 57-65.

Minshall, G. W., S. A. Thomas, et al. (2000). "Physical factors influencing fine organic particle transport and deposition in streams." Journal of the North American Benthological Society **19**(1): 42370.

Neal, C., W. A. House, et al. (1998). "An assessment of excess carbon dioxide partial pressures in natural waters based on pH and alkalinity measurements." Science of the Total Environment **210**(1-6): 173-185.

Ohno, T. (2002). "Fluorescence inner-filtering correction for determining the humification index of dissolved organic matter." Environmental Science & Technology **36**(4): 742-746.

Oquist, M. G., M. Wallin, et al. (2009). "Dissolved Inorganic Carbon Export Across the Soil/Stream Interface and Its Fate in a Boreal Headwater Stream." Environmental Science & Technology **43**(19): 7364-7369.

Osawa, T., H. Mitsuhashi, et al. (2010). "Enhanced Diversity at Network Nodes: River Confluences Increase Vegetation-Patch Diversity." The Open Ecology Journal **3**: 48-58.

Owen, D. M., G. L. Amy, et al. (1995). "NOM Characterization and Treatability." A W W A **87**(1): 46-63.

Parlanti, E., K. Worz, et al. (2000). "Dissolved organic matter fluorescence spectroscopy as a tool to estimate biological activity in a coastal zone submitted to anthropogenic inputs." Organic Geochemistry **31**(12): 1765-1781.

Peuravuori, J. and K. Pihlaja (1997). "Molecular size distribution and spectroscopic properties of aquatic humic substances." Analytica Chimica Acta **337**(2): 133-149.

Power, M. E. and W. E. Dietrich (2002). "Food webs in river networks." Ecological Research **17**: 451-471.

Quinn, G. P. and M. J. Keough (2002). Experimental design and data analysis for biologists. Cambridge, UK, Cambridge University Press.

Raymond, P. A., C. J. Zappa, et al. (2012). "Scaling the gas transfer velocity and hydraulic geometry in streams and small rivers." Limnology and Oceanography: Fluids and Environment **2**: 1-14.

Ripley, B. D. (1996). Pattern Recognition and Neural Networks. Cambridge, U.K., Cambridge University Press.

Seitzinger, S. P., H. Hartnett, et al. (2005). "Molecular-level chemical characterization and bioavailability of dissolved organic matter in stream water using electrospray-ionization mass spectrometry." Limnology and Oceanography **50**(1): 1-12.

Stedmon, C. A. and R. Bro (2008). "Characterizing dissolved organic matter fluorescence with parallel factor analysis: a tutorial." Limnology and Oceanography Methods **6**: 572-579.

Stedmon, C. A. and S. Markager (2005). "Resolving the variability in dissolved organic matter fluorescence in a temperate estuary and its catchment using PARAFAC analysis." Limnology and Oceanography **50**(2): 686-697.

Stumm, W. and J. J. Morgan (1996). Aquatic Chemistry - Chemical Equilibria and Rates in Natural Waters. New York, John Wiley & Sons.

Thurman, E. M. (1985). Developments in biogeochemistry: organic geochemistry of natural waters. Dordrecht, The Netherlands, Martinus Nijhoff and Dr W. Junk Publishers.

Twardowski, M. S., E. Boss, et al. (2004). "Modeling the spectral shape of absorption by chromophoric dissolved organic matter." Marine Chemistry **89**(1-4): 69-88.

Vannote, R. L., G. W. Minshall, et al. (1980). "The river continuum concept." Canadian Journal of Fisheries and Aquatic Sciences **37**: 130-137.

Vodacek, A., M. D. De Grandpre, et al. (1997). "Seasonal variation of CDOM and DOC in the Middle Atlantic Bight: Terrestrial inputs and photooxidation." Limnology and Oceanography **42**: 674-686.

Wallin, M., I. Buffam, et al. (2010). "Temporal and spatial variability of dissolved inorganic carbon in a boreal stream network: Concentrations and downstream fluxes." Journal of Geophysical Research-Biogeosciences **115**: 1-12.

Wallin, M., M. Öquist, et al. (2011). "Spatiotemporal variability of the gas transfer coefficient (KCO2) in boreal streams; implications for large scale estimates of CO2 evasion." Global Biogeochemical Cycles **25**(GB3025): 14.

Wanninkhof, R., P. J. Mulholland, et al. (1990). "Gas-exchange rates for a 1st-order stream determined with deliberate and natural tracers." Water Resources Research **26**(7): 1621-1630.

Weishaar, J. L., G. R. Aiken, et al. (2003). "Evaluation of specific ultraviolet absorbance as an indicator of the chemical composition and reactivity of dissolved organic carbon." Environmental Science & Technology **37**(20): 4702-4708.

Wilson, H. F. and M. A. Xenopoulos (2008). "Ecosystem and seasonal control of stream dissolved organic carbon along a gradient of land use." Ecosystems **11**(4): 555-568.

Wilson, H. F. and M. A. Xenopoulos (2008). "Effects of agricultural land use on the composition of fluvial dissolved organic matter." Nature Geoscience **2**: 37-41.

Zeng, F.-W. and C. A. Masiello (2010). "Sources of CO2 evasion from two subtropical rivers in North America." Biogeochemistry(100): 211-225.

Zsolnay, A., E. Baigar, et al. (1999). "Differentiating with fluorescence spectroscopy the sources of dissolved organic matter in soils subjected to drying." <u>Chemosphere</u> **38**(1): 45-50.